QUARTERLY JOURNAL OF THE ROYAL METEOROLOGICAL SOCIETY
*Q. J. R. Meteorol. Soc.* **133**: 227–250 (2007)
Published online in Wiley InterScience
(www.interscience.wiley.com) DOI: 10.1002/qj.6

# Critical re-evaluation of the bulk transfer coefficient for sensible heat over the ocean during unstable and neutral conditions

Ann-Sofi Smedman,* Ulf Högström, Erik Sahlée and Cecilia Johansson
*Department of Earth Sciences, Uppsala University, Sweden*

**ABSTRACT:** A new analysis of the neutral heat transfer coefficient $C_{HN}$ on data from Östergarnsholm is presented, which is primarily based on a limited set of measurements with the very accurate MIUU (Meteorological Institute of the University of Uppsala) instrument, but with additional information from an extensive set of measurements with Solent sonic R2. Sonic data are, however, used with great caution, since for wind speed $U$ above 10 m s$^{-1}$, a strongly wind-speed-dependent correction is shown to be required. This error is roughly proportional to $(U - 10)$ for sea–air temperature differences less than 4–5 K. For a larger temperature difference, no correction appears to be necessary in the wind speed range 10–15 m s$^{-1}$.

We infer from our data that for conditions when unstable and near-neutral conditions prevail, measurements of the sea surface – air temperature difference are accurate to within 0.1 K at our site. This means that data for a range of relatively small temperature differences (0.5–1.5 K) which were often rejected in previous studies could be retained. It is observed that a rapid increase of $C_H$ and $C_{HN}$ occurs in that range.

For wind speed above 10 m s$^{-1}$, $C_{HN}$ is observed to increase rapidly with $U_{10}$. During those conditions, the wave field at the site is known to have characteristics very similar to those in deep-sea conditions. In a previous analysis of data from Östergarnsholm, it was speculated that observed high $C_{HN}$ values could be due to spray. Calculations with a spray model showed, however, conclusively that for wind speeds less than 14 m s$^{-1}$, the spray effect on the sensible heat flux is expected to be small. The high $C_{HN}$ values must instead be due to dynamic effects.

It is demonstrated that when the Obukhov length $L$ is less than about $-150$ m a regime with very specific characteristics ensues. This regime is dominated by surface-layer scale eddies, which cause Monin–Obukhov relations for the exchange of sensible heat to break down. The characteristics of this surface-layer regime are treated in detail in the companion paper.

The rise of $C_{HN}$ with wind speed is shown to be closely related to a corresponding increase of $z_{0T}$ with roughness Reynolds number for winds above 10 m s$^{-1}$. This means that during those conditions, traditional surface renewal theory for heat is no longer valid. It is suggested that this, in turn, is a result of increasing importance of wave-breaking with increasing wind and with a possible link to processes in near-surface atmospheric layers in the regime with $-L > 150$ m. 

KEY WORDS sensible heat flux; marine boundary layer; turbulent exchange

*Received 17 October 2005; Revised 3 October 2006*

## 1. Introduction

Correct parametrization for the exchange of sensible and latent heat at the surface of the ocean is crucial for climate modelling and weather forecasts. Many dedicated field experiments with the aim to quantify the relationships between fluxes and bulk variables have been conducted during the last three or more decades. Nevertheless, as illustrated vividly in Brunke *et al.* (2003), who compared 12 flux algorithms against data from 12 oceanic field experiments, there still remains considerable uncertainty concerning the corresponding bulk-flux relations, in particular for the flux of sensible heat for which some studies suggest a dependence of the exchange coefficient on wind speed whereas others find no such variation. The present paper is devoted to a reanalysis of the bulk flux relationships for sensible heat based on data from the Östergarnsholm marine field station in the Baltic Sea, whereas in a forthcoming paper, Sahlée *et al.* (2007), the corresponding relationships for the flux of latent heat is presented.

Results from an analysis of the flux of sensible heat based on data from the Östergarnsholm station were presented by our group quite recently in this journal, Guo Larsén *et al.* (2004), GL2004 below. Data for the neutral bulk exchange coefficient $C_{HN}$ appeared to follow the general trend predicted by the COARE2.0 algorithm (Fairall *et al.*, 1996b) for unstable stratification but with some high values in the wind speed range 10–14 m s$^{-1}$, which were speculatively interpreted as being due to spray. Later, simulations with the spray model of

* Correspondence to: Ann-Sofi Smedman, Department of Earth Sciences, Uppsala University, Sweden.
E-mail: ann-sofi.smedman@met.uu.se

Andreas (2004) by Sahlée *et al.* (2007), showed that the expected contribution of spray to the flux of sensible heat in this wind speed range is only 5–10%. This finding is also in general agreement with the conclusions from the HEXOS experiment, Decosmo *et al.* (1996); cf. also Andreas and DeCosmo (2002). In addition, a close look at the plot of $C_{\mathrm{HN}}$ against wind speed in GL2004, Figure 11 of that paper, reveals that all the high $C_{\mathrm{HN}}$ values were obtained with the MIUU (Meteorological Institute of the University of Uppsala) instrument and turned out to be considerably higher than the corresponding values obtained for the same wind speed with the Solent sonic R2 instrument. This is particularly challenging as we know that the MIUU instrument can be considered as a reference instrument for atmospheric turbulence measurements (Högström and Smedman, 2004 and the appendix to the present paper). These observations prompted us to take another look at the data. As illustrated below, giving due weight to the data taken with the MIUU instrument and carefully screening the R2 data for erroneously low sensible heat flux values in high winds, and also relaxing on the constraint imposed on the air–sea temperature difference imposed in GL2004, gives a very different end result: $C_{\mathrm{HN}}$ turns out to be a strong function of wind speed.

Section 2 presents the theoretical framework for the analysis, section 3 the site and measurements. Section 4 is a critical comparison of the heat flux estimates obtained with the two types of turbulence instruments employed, the Gill Solent sonic anemometer and the MIUU instrument. In section 5 the results are presented, and in section 6 the new findings are discussed in the light of previously published results on $C_{\mathrm{HN}}$. Finally, section 7 gives the conclusions.

## 2. Theoretical framework

The bulk exchange coefficient for the sensible heat flux $C_H$ is defined:

$$C_{\mathrm{H}} = \overline{w'\theta'}/(U_{10} - U_{\mathrm{s}})(\Theta_{\mathrm{w}} - \Theta_{10}), \tag{1}$$

where

$\overline{w'\theta'}$ = the kinematic heat flux at the surface (m s$^{-1}$K)
$U_{10}$ = mean wind speed at 10 m height above the water surface (m s$^{-1}$)
$U_{\mathrm{s}}$ = mean wind speed at the water surface (m s$^{-1}$)
$\Theta_{\mathrm{w}}$ = potential temperature of the water surface (K)
$\Theta_{10}$ = potential temperature at 10 m above the water surface (K)

Here it is assumed that $\overline{w'\theta'}$ is approximately constant throughout the atmospheric surface layer (see section 3 for a discussion). In the absence of a large-scale surface current, $U_{\mathrm{s}}$ is equal to the drift velocity, which is about 2% of the wind speed, so that in practice we set $U_{\mathrm{s}} = 0$.

Provided Monin–Obukhov (MO) theory is valid (cf. section 5), we have, for the dimensionless wind profile and temperature profile respectively:

$$\phi_m(z/L) = \frac{\kappa z}{u_*} \cdot \frac{\partial U}{\partial z}, \tag{2a}$$

$$\phi_H = \frac{\kappa z}{T_*} \cdot \frac{\partial \Theta}{\partial z}, \tag{2b}$$

where $u_* = \sqrt{-\overline{u'w'}}$ = the friction velocity (m s$^{-1}$), $T_* = -\overline{w'\theta'}/u_*$ = the temperature scale (K), and $L$ the Obukhov length-scale:

$$L = -\frac{{u_*}^3 T_0}{\kappa g \overline{w'\theta_{\mathrm{v}}'}}. \tag{3}$$

Here $T_0$ is the mean temperature of the surface layer (K), $\kappa$ is von Karman's constant = 0.40 and $g$ the acceleration of gravity = 9.81 m s$^{-2}$. $\overline{w'\theta_{\mathrm{v}}'}$ is the flux of virtual potential temperature, which is very nearly the same as the flux of sonic temperature, obtained directly from the sonic (Dupuis *et al.*, 1997). The MIUU instrument gives $\overline{w'\theta'}$, and the following relation (Lumley and Panofsky, 1964) is used to obtain $\overline{w'\theta_{\mathrm{v}}'}$:

$$\overline{w'\theta_{\mathrm{v}}'} = \overline{w'\theta'}(1 + 0.07/\beta), \tag{4}$$

where

$$\beta = H/E\lambda \approx c_p(\Theta_{\mathrm{w}} - \Theta_{10})/\lambda(q_{\mathrm{s}} - q_{10}), \tag{5}$$

$\beta$ = the Bowen ratio = and $H$ = the flux of sensible heat (W m$^{-2}$), $E\lambda$ = the flux of latent heat (W m$^{-2}$), $c_p$ = specific heat at constant pressure and $\lambda$ = specific heat of vaporization; $q_{\mathrm{s}}$ is saturation specific humidity (kg $H_2O$/kg air) at temperature $\Theta_{\mathrm{w}}$ and $q_{10}$ = specific humidity at 10 m. The approximation in (5) requires that the dimensionless profile function for humidity, $\phi_q$ equals $\phi_H$, which is in agreement with recent findings of Edson *et al.* (2004).

Integration of Equations (2a) and (2b) gives respectively:

$$U(z) = \frac{u_*}{\kappa}\{\ln(z/z_0) - \psi_m(z)\}, \tag{6}$$

$$\Theta(z) - \Theta_{\mathrm{w}} = \frac{T_*}{\kappa}\{\ln(z/z_{0T}) - \psi_h(z)\}. \tag{7}$$

Here $z_0$ and $z_{0T}$ are the roughness lengths for momentum and heat, i.e. the heights where $U = U_{\mathrm{s}} = 0$ and $\Theta = \Theta_{\mathrm{s}}$ respectively and

$$\psi_m(z) = \int_0^{z/L} \{1 - \phi_m(\zeta)\}/\zeta^{-1} d\zeta, \tag{8}$$

$$\psi_h(z) = \int_0^{z/L} \{1 - \phi_H(\zeta)\}/\zeta^{-1} d\zeta. \tag{9}$$



DOI: 10.1002/qj

Combining Equations (1), (6) and (7) gives the following expression for $C_H$:

$$C_H = \frac{\kappa^2}{\{\ln(z/z_0) - \psi_m\}\{\ln(z/z_{0T}) - \psi_h\}}. \quad (10)$$

In neutral conditions, $z/L = 0$ and $\psi_m = \psi_h = 0$, which enables definition of a neutral exchange coefficient for sensible heat $C_{HN}$:

$$C_{HN} = \frac{\kappa^2}{\{\ln(z/z_0)\}\{\ln(z/z_{0T})\}}. \quad (11)$$

Note, that provided $\phi_m(z/L)$ is known, $z_0$ can be derived with Equation (6) from measurements of wind speed at 10 m $U_{10}$ and friction velocity $u_*$. In a similar way, $z_{0T}$ can be obtained with Equation (7) from measurements of $(\Theta_w - \Theta_{10})$ and $T_*$ provided $\phi_H(z/L)$ is known. Below, expressions for $\phi_m(z/L)$ for unstable conditions $(z/L < 0)$ based on recent studies from Östergarnsholm will be given. The situation for $\phi_H(z/L)$ will be discussed in section 5.

In a series of papers from the Östergarnsholm project, e.g. Rutgersson *et al.* (2001), Sjöblom *et al.* (2003a) and GL2004, it has been demonstrated how $\phi_m(z/L)$ is influenced by surface wave effects. Similar to what was done in GL2004, we define $\phi_m(z/L)$-functions for three wave age ranges, defined in terms of $c_0/U_{10}$, where $c_0$ = phase speed of dominant waves (m s$^{-1}$):

(I) Growing sea, $c_0/U_{10} < 0.8$,

$$\phi_m = (1 - 19z/L)^{-1/4}, \quad (12)$$

which is the expression recommended by Högström (1996) for general use over land.

(II) Mixed seas (or mature sea), $0.8 < c_0/U_{10} < 1.2$,

$$\phi_m = 1 - (-2z/L)^{1/2}, -0.5 < z/L < 0, \quad (13)$$

$$\phi_m = 0, \mathrm{z}/L < -0.5, \quad (14)$$

(III) Swell, $c_0/U_{10} > 1.2$,

$$\phi_m = 1 - (-3z/L)^{1/2}, -1 < z/L < 0 \quad (15)$$

$$\phi_m = -0.73, z/L < -1. \quad (16)$$

Note that Equations (15) and (16) were obtained for wave-following swell, valid for a wind/wave angle of less than 30° and for conditions when the wave spectra have a single peak. Such conditions are typical for the Östergarnsholm site and probably for the Baltic Sea at large (Guo Larsén, 2003) but not necessarily for deep sea conditions, cf. section 6.

## 3. Site and measurements

### 3.1. The measurement site

The data for this study were obtained at the Östergarnsholm field station, situated about 4 km east of the big island Gotland in the Baltic Sea (57°27′N, 18°59′E), see e.g. GL2004 for a map. Östergarnsholm is a very low island with no trees but covered with short grass and herbs. At the southernmost tip of the island a 30 m instrumented tower has been erected. The tower base is situated 1.4 m above mean sea level. The variation of water level in this part of the Baltic Sea is about ±0.5 m and the heights to the different measuring levels have been corrected using water level measurements at Visby harbour, situated at the west coast of the island of Gotland. The distance from the tower to the shore line is between 5 and 20 m in the undisturbed sector (80°–220°).

The sea floor around the island has a slope of about 1 : 30 close to the shore. At about 10 km from the peninsula the water depth is 50 m, reaching below 100 m farther out. In Smedman *et al.* (1999) the possible influence of limited water depth on the tower measurements was studied in detail. Flux footprint calculations were done, showing that the turbulence instruments 'see' areas far upstream of the island. But still sufficiently long waves 'feel' the presence of the bottom, implying that peak wave phase speed $c_0$ must be calculated using the general dispersion relation:

$$c_0 = \frac{g}{\omega_0} \tanh\left(\frac{\omega_0 h}{c_0}\right), \quad (17)$$

where $\omega_0$ is frequency (radian·s$^{-1}$), $h$ the water depth (m) and $g$ acceleration of gravity (m s$^{-2}$).

Taking the 'footprint weighting function' $F(z)$ from Equation (A7) of appendix A of Smedman *et al.* (1999), it is possible to calculate a weighted mean phase speed

$$\langle c_0 \rangle = \int_0^\infty F(x, z) c_0(x) \mathrm{d}x. \quad (18)$$

Whenever $c_0$ is used in this paper, it has been calculated with Equation (18). Smedman *et al.* (1999) found that, although the phase speed of the relatively long waves was indeed influenced by shallow water effects, little effect on the turbulence structure in the atmospheric surface layer was observed. In Smedman *et al.* (2003) a comparison was made of roughness length $z_0$ (m) for pure wind sea conditions (young waves) from Östergarnsholm and from deep sea expeditions. It showed that the Östergarnsholm data agree very well with the corresponding calculations presented in Drennan *et al.* (2003), based on deep sea data.

A Waverider buoy (owned and run by the Finnish Institute of Marine Research, FIMR) is moored at 36 m depth ~4 km from the tower in the direction 115°, representing the wave conditions in the upwind fetch area (see below).

### 3.2. Profile instrumentation

During the time period May 1995 – July 2002, the 30 m tower at Östergarnsholm was instrumented with



DOI: 10.1002/qj

slow-response profile sensors of in-house design for temperature (Högström, 1988) and for wind speed and direction at 5 heights (new, slightly modified instrumentation was later installed on the tower and measurements were resumed, but data from that later period are not used here). The accuracy of the anemometers is 0.2 m $s^{-1}$, and as shown in Smedman *et al.* (1991), it has negligible over-speeding (i.e. because of careful design of the small and light anemometer cups, the instrument has nearly linear response to velocity changes). Air temperature was measured with platinum 500 ohm resistance sensors in aspirated radiation shields as consecutive differences between levels and with an additional sensor at the lowest level for 'absolute' temperature. The estimated accuracy in the temperature differences measurements is ±0.02 K (Smedman and Högström, 1973; Högström, 1988; see also section 5). Humidity was measured at one level (8 m) with a Rotronic sensor.

### 3.3. Turbulence instrumentation

The 30 m tower is equipped with Solent sonic 1012R2 anemometers at three heights: 9, 16 and 25 m above the tower base, which is $1.4 \pm 0.4$ m above the water surface. This instrumentation has been employed on a semi-continuous basis since May 1995. During intensive measuring campaigns, we have also employed a MIUU turbulence instrument at the lowest turbulence measurement level ($10.4 \pm 0.4$ m above the water surface) for a period of one or two weeks each time.

The MIUU instrument is basically a wind-vane-mounted three-component hot-film instrument with additional platinum sensors for temperature and wet-bulb temperature, see Figure A.1 in the appendix. The dry-bulb sensor consists of a long (15 cm) platinum wire with a diameter of 15 μm, which gives a time constant of 0.005 s. Note that salinity in the Baltic Sea is very low, about 6 ppt around Östergarnsholm. This means that we never have problems with salt contamination of the Pt wire as often reported when such measurements are attempted over the deep sea, where salinity is about six times higher. The low salinity is also crucial for successful use of the hot film technique. The design properties and performance of the MIUU instrument are treated in detail in the appendix. In section 4.1 systematic comparison of heat flux estimates obtained with the MIUU instrument and with the sonic is performed.

Throughout this paper, basic averaging time for all turbulence statistics (from the sonics as well as from the MIUU instrument) is 60 minutes.

### 3.4. Data selection

General criteria for data selection are:

(i) Wind from the sector with undisturbed long fetch (>150 km), 80°–220°;
(ii) complete data coverage, including wave data (the Waverider buoy is removed during periods with risk for damage by ice);
(iii) positive sensible heat flux and sea surface-air temperature difference, $\Delta\Theta = \Theta_w - \Theta_{10}$;
(iv) approximate constancy with height of virtual temperature flux and momentum flux between 10 and 26 m.

Two datasets were selected:

A. Data from a period in October 1999 with 66 hours of data taken with the MIUU instrument at the 10 m level. During the time period from 1100 h, 21 October to 0800 h, 24 October 1999, conditions were ideally suited for the present study: stratification was unstable, the wind speed varied between about 4 m $s^{-1}$ and 14 m $s^{-1}$ and $\Delta\Theta$ between less than 1 K and about 5 K, thus covering a fairly wide parameter range.
B. R2 data from the period May 1995 to August 1998 plus a period of six months from 2001. For this basic dataset, which includes in all 1195 hours of data that fulfil the general criteria given above, mean ratios of sensible heat flux between 10 and 16 m and between 16 and 26 m were found to deviate by less than 5% from unity; a similar result was obtained for the corresponding ratios of $u_*$. A subset of 525 data which fulfill the criterion $\overline{w'\theta'} > 0.02$m $s^{-1}$ K is used in most of the analyses below, the reason for introducing this criterion being a desire to reduce scatter.

In Figure 1 has been plotted the quantity $\overline{w'\theta'}/U_{10}$ against $\Delta\Theta = (\Theta_w - \Theta_{10})$ for the entire dataset (thus including corrected high-wind cases). Here, $\Theta_w$ has been taken from the Waverider buoy at about 0.5 m below the water surface and $\Theta_{10}$ from the tower. $\overline{w'\theta'}$ has been taken from the sonic data for $\overline{w'\theta_v'}$, after application of Equations (4) and (5). Regression of all the data gives a line that intercepts the $x$-axis at 0.04 K. We take this result to imply that our measurements of $\Delta\Theta$ are indeed representative of the true sea surface – air temperature difference. The very close proximity to a (0,0)-intercept is probably fortuitous, but Rutgersson *et al.* (2001) employed the algorithm developed by Fairall *et al.* (1996a) and found the 'warm layer effect' to be very small, and the 'cool skin effect' to be about 0.1 °C at 10 m $s^{-1}$ on the average. $\Theta_w$ and $\Theta_{10}$ are measured at locations 3.5 km apart, so coexistence of positive heat flux at the surface with deep vertical mixing in the upper part of the ocean is the likely explanation for the good agreement. Such deep vertical mixing is indeed known to prevail in the Baltic Sea during autumn when positive heat flux dominates. The corresponding plot of data from stable conditions (not shown here) gives a very different picture compared to that shown in Figure 1. Instead of converging toward (0,0), the plot indicates an uncertainty of 0.5–1.0 K. Part of this increased scatter is believed to be due to much more patchy sea surface temperature during conditions with stable stratification both in the air and in the water. In GL2004 data with $\Delta\Theta < 1.5$ K were



DOI: 10.1002/qj

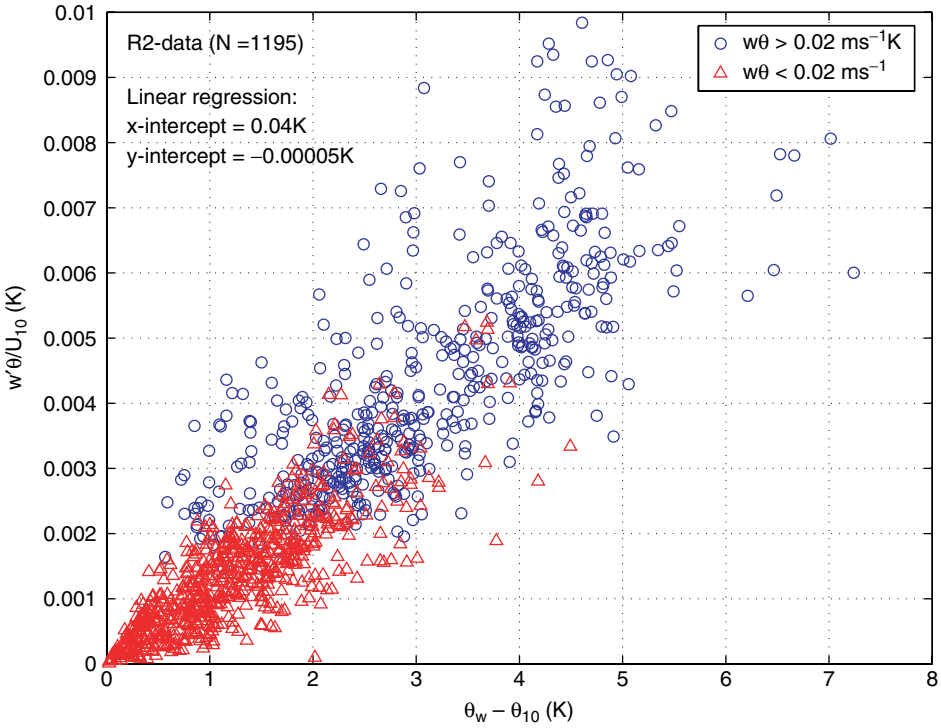


Figure 1. Plot of $(\overline{w'\theta'})/U_{10}$ for all R2 data (60-minute mean values) against the sea–air temperature difference, $\Theta_w - \Theta_{10}$, where $\Theta_w$ was obtained on the wave rider buoy at 0.5 m depth and $\Theta_{10}$ from 10 m height on the Östergarnsholm tower. This figure is available in colour online at www.interscience.wiley.com/qj

rejected. Considering Figure 1, it is reasonable to retain data with $\Delta\Theta > 0.5$ K.

## 4. Comparison of heat flux estimates obtained with sonic anemometers and with the MIUU instrument

A field intercomparison test of flux measurements with the Solent R2 and the very similar Solent R3 and the MIUU instrument has been reported in Högström (2001) and in Högström and Smedman (2004). It was demonstrated that the performance of the MIUU instrument in a side-by-side test of 3 MIUU instruments was such that it is justifiable to denote this instrument a 'reference instrument' – for a more detailed discussion, see appendix.

Of particular interest for the present study is the ability of the sonic instruments to record the sensible heat flux. Two tests are of relevance here: (i) A MIUU-instrument and a sonic R3 instrument placed at the end of 5 and 4 m long booms at 10 m on the Östergarnsholm tower during October 1999, the distance between the instruments being 1.3 m, and (ii) an R2 and an R3-instrument placed at the end of the same two booms during December 1999.

In test (i) the fluxes of potential temperature, $\overline{w'\theta'}$ were compared. The R3 data were corrected for the cross-wind correction in the instrument electronics and the resulting $\overline{w'\theta_v'}$ values were transformed to $\overline{w'\theta'}$ with Equations (4) and (5).

In test (ii) $\overline{w'\theta_v'}$ values were compared directly. Then R2 data were subjected to cross-wind correction according to Kaimal and Gaynor (1991).

For test (ii) the difference $(\overline{w'\theta_v'})_{R3} - (\overline{w'\theta_v'})_{R2}$ was plotted against wind speed. The 675 half-hour data cover the range $2 < U_{10} < 22$ m s$^{-1}$. The plot (Figure 26 in Högström, 2001) shows that the scatter increases very much for $U_{10} > 10$ m s$^{-1}$, but the mean of the difference does not vary with wind speed and is very close to zero. This shows that the R2 and R3 instruments appear not to differ in their ability to record the heat flux, which means that we expect test (i) of R3 against the MIUU instrument (see below) to be equally valid for R2.

The open circles in Figure 2 are $(\overline{w'\theta'})_{MIUU}/(\overline{w'\theta'})_{R3}$ plotted as a function of wind speed from test (i). Filled circles are wind speed bin averages of the same data. For $U_{10} < 10$ m s$^{-1}$ the mean ratio is close to unity, but for higher wind speed it increases significantly. As the scatter among the values with $U_{10} > 10$ m s$^{-1}$ is very large, it is difficult to estimate a reliable trend. In Figure 1 a tentative fit is given by the line

$$y = 1.0 + 0.2(U_{10} - 10), \quad 10 < U_{10} < 13 \text{ m s}^{-1}, \tag{19}$$

where $y = (\overline{w'\theta'})_{MIUU}/(\overline{w'\theta'})_{R3}$. Figure 3 shows a plot of $C_H$ against $U_{10}$ based on uncorrected R2 data (grey dots) and data obtained with the MIUU instrument (circles). Here, and later on in the text, 'uncorrected R2 data' refers to $\overline{w'\theta'}$ data which have not been subjected to correction with Equation (19). In order to reduce the scatter in the plot, only R2 data with $\overline{w'\theta'} > 0.02$ m s$^{-1}$ K have been included, but the result when this restriction is not made is exactly the same in the mean. Also shown in the figure are bin average means over 0.5 m s$^{-1}$ intervals for R2



DOI: 10.1002/qj

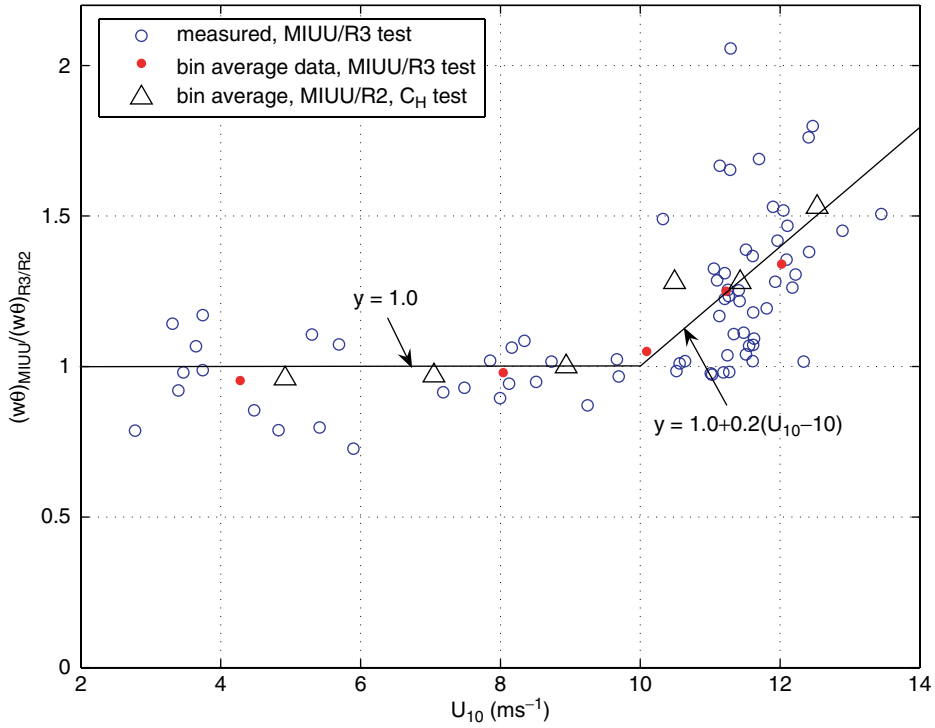


Figure 2. The ratio $(\overline{w'\theta'_v})_{MIUU}/(\overline{w'\theta_v'})_{R3/R2}$ plotted against wind speed at 10 m, obtained from: (i) the field intercomparison test of the MIUU instrument and R3 at Östergarnsholm, October 1999, open and closed circles; (ii) MIUU/R2 $C_H$-test, triangles. Best-fit lines have been drawn for two intervals: $2 < U_{10} < 10$ m s$^{-1}$ and $U_{10} > 10$ m s$^{-1}$. This figure is available in colour online at www.interscience.wiley.com/qj

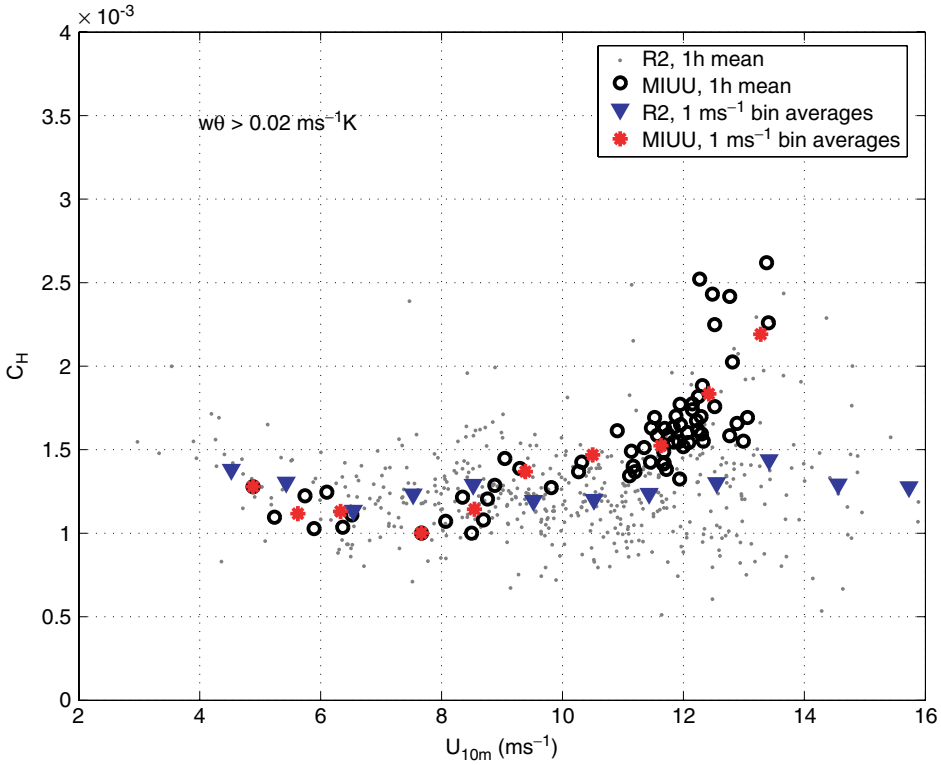


Figure 3. $C_H$ (60-minute mean values) plotted against $U_{10}$. The R2 data (grey dots) are based on a sub-dataset with $\overline{w'\theta'} > 0.02$ m s$^{-1}$ K and have not been corrected for the wind speed effect on the heat flux. Black circles are derived from MIUU data. Bin averages at 1 m s$^{-1}$ intervals have also been included for both datasets (see insert legend). This figure is available in colour online at www.interscience.wiley.com/qj



DOI: 10.1002/qj

(triangles) and for the MIUU instrument (bullets). For $U_{10} < 10$ m s$^{-1}$ there is not much variation in the mean, and R2 and MIUU bin averages agree, but for higher wind speed, the MIUU data are systematically higher than the R2 data and increasingly so with increasing $U_{10}$. From the data plotted in this figure, it is possible to derive bin average values over intervals of $U_{10}$ for MIUU data and R2 data separately. As, for each such group, mean $(\Theta_w - \Theta_{10})$ values do not differ much, it is possible to obtain approximate ratios of $\overline{w'\theta'}$, i.e.:

$$y = (C_H)_{MIUU}/(C_H)_{R2} \approx (\overline{w'\theta'})_{MIUU}/(\overline{w'\theta})_{R2}.$$

Data derived from Figure 3 in this way are plotted as triangles in Figure 2. It is clear that these data come very close to the two lines drawn in the figure, i.e. $y = 1.0$ for $U_{10} < 10$ m s$^{-1}$ and Equation (19) for $10 < U_{10} < 13$ m s$^{-1}$.

Figure 4(a), (b) and (c) show $C_H$ plotted as function of $\Delta\Theta$ for, respectively $U_{10} > 12$ m s$^{-1}$, Figure 4(a); $10 < U_{10} < 12$ m s$^{-1}$, Figure 4(b); and $U_{10} < 10$ m s$^{-1}$, Figure 4(c). For the R2 data, 0.5 K bin averages have been derived. Tentative lines have been fitted by eye to help visualize the trend of the R2 and MIUU datasets in Figure 4(a) and (b) and for R2 in Figure 4(c). Two things are evident from Figure 4(a) and (b): (i) mean R2 data are systematically lower than corresponding MIUU data for most of the $\Delta\Theta$ range encountered in the dataset; (ii) in Figure 4(a) there is an upward trend in the R2 data for $\Delta\Theta > 4$ K and a corresponding increase in Figure 4(b) for $\Delta\Theta >$ c. 2.7 K. Thus, for $U > 10$ m s$^{-1}$, there appears to be a limit for $\Delta\Theta$ above which R2 and MIUU data seem to converge.

For $U < 10$ m s$^{-1}$, Figure 4(c), the situation is entirely different: no variation in $C_H$ derived from R2 measurements is seen in the mean over the range $0.5\ K < \Delta\Theta < 9$ K; MIUU data for this wind speed range happen to be restricted to a narrow range in $\Delta\Theta$. But the mean value of $C_H$ for the MIUU data for this wind speed range is within 1% of the corresponding mean value obtained by the R2 instrument for the entire $\Delta\Theta$ range.

Figure 5(a), (b), (c) and (d) compares temperature spectra obtained with the R3 and the MIUU instruments, Figure 5(a) and (c), and corresponding $w\theta$ co-spectra, Figure 5(b) and (d), for two cases during the MIUU/R3 intercomparison test. Figure 5(a) and (b) shows spectra for a case with $U = 7.9$ m s$^{-1}$ and $\Delta\Theta = 5.4$ K; Figure 5(c) and (d) is for a period with mean $U = 12.3$ m s$^{-1}$ and $\Delta\Theta = 1.7$ K ($N = 7$). In the case of Figure 5(a) and (b), there is broad agreement between the two curves in each of the graphs. This contrasts sharply to Figure 5(c) and (d), which shows gross disagreement between the plots from the two instruments in both temperature spectrum, 5(c), and co-spectrum, 5(d). The R3 temperature spectrum has a minimum where there is a maximum in the corresponding MIUU spectrum around $n = 0.3$ hertz and continues to rise steadily with increasing frequency, whereas the MIUU spectrum shows an expected $-2/3$ fall-off (except for the highest frequency). The MIUU co-spectrum has a pronounced maximum at $n = 0.3$ hertz, but the R3 co-spectrum has a rather flat shape. For a detailed discussion of the spectra and co-spectra, cf. Smedman *et al.* (2007).

Figure 6(a) and (b) compares mean normalized $w\theta$ co-spectra from R2 and MIUU for two groups of data: Figure 6(a), $U_{10} < 7$ m s$^{-1}$ and $\Delta\Theta > 3$ K ($N_{R2} = 21$ and $N_{MIUU} = 6$) and Figure 6(b), $U_{10} > 10$ m s$^{-1}$ and $\Delta T < 2$ K ($N_{R2} = 51$ and $N_{MIUU} = 10$). Again, it is seen that good agreement is obtained for the case with low wind and large temperature difference, 6(a), and gross disagreement in the high wind, low $\Delta\Theta$ case. Figure 6(b) is very similar to the corresponding plot from the MIUU/R3 test, Figure 5(d). In both cases, the MIUU curve shows a pronounced high-frequency peak, which contrasts strongly to the rather flat R2 or, as the case may be, R3 shape for the co-spectrum. Thus, in the case of $U > 10$ m s$^{-1}$, the R2 and R3 sonics miss much of the co-spectral energy contained at relatively high frequencies, and hence the recorded flux is underestimated as noted above.

The wind-speed-dependent error in the R2 (and R3) estimates of the heat flux is remarkable, not the least as this or similar instruments have been used in many air–sea interaction studies in the past, cf. section 6.

The same behaviour was previously observed by Grelle and Lindroth (1996), who used R2 instruments for measuring the sensible heat flux on a high tower over a forest. They had employed a Pt-8 temperature sensor together with their R2 instrument and found that the heat flux derived with the sonic instrument alone and with the sonic only for vertical velocity and the Pt-sensor for temperature agreed well for wind speeds up to about 10 m s$^{-1}$ but deviated strongly with increasing wind. Thus, their Figure 5a illustrates the situation during a daytime summer-day run with high wind. For this case, the heat flux derived with the sonic plus the Pt-sensor is positive and consistently higher than the heat flux derived from the sonic alone, i.e. exactly in agreement with the present findings. (Note: in stable air and with $U_{10} > 10$ m s$^{-1}$, the authors find that the magnitude of the sonic-alone heat flux, $H_{sonic}$ is larger than the sonic plus Pt8 heat flux, $H_{sonic+Pt8}$, e.g. $H_{sonic} = -50$ W m$^{-2}$ and $H_{sonic+Pt8} = -20$ W m$^{-2}$, i.e. for all stability and $U_{10} > 10$ m s$^{-1}$, $H_{sonic} < H_{sonic+Pt8}$.) Grelle and Lindroth (1996) comment on their findings: 'We are not able to explain the source of these differences at the current stage, but they are likely caused by oscillations and deformations of the sonic probe.... Intercomparisons with USAT-3 (METEK, Hamburg, Germany) and Kaijo-Denki sonic...prior to this study showed basically the same behaviour and even similar threshold wind speeds of all systems. This means that as long as no appropriate correction can be applied on the sound virtual temperature, reliable heat flux point measurements at high wind speeds can only be carried out by means of fast temperature sensors.'

Achim Grelle (personal communication, 2006) refers to discussions with Niels-Otto Jensen and Niels Mortensen at Risö Laboratory, Denmark. They are of the opinion



DOI: 10.1002/qj

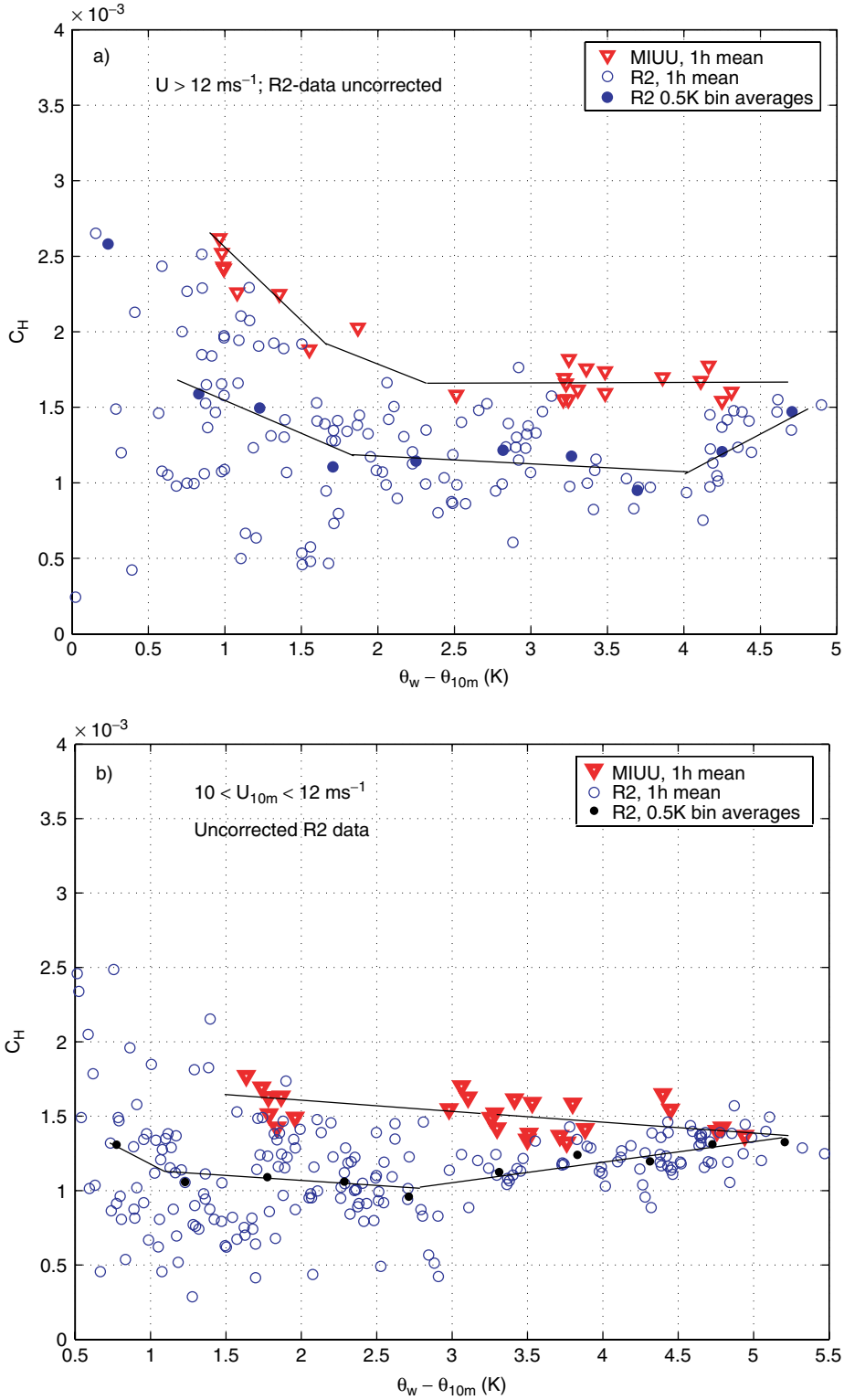


Figure 4. $C_H$ derived with the heat flux from the MIUU instrument, triangles and from uncorrected R2 data, open circles, plotted against $\Theta_w - \Theta_{10}$, for cases with (a) $U_{10} > 12$ m s$^{-1}$, (b) $10 < U_{10} < 12$ m s$^{-1}$ and (c) $U_{10} < 10$ m s$^{-1}$. Bin average values at 0.5 K intervals have been plotted for the R2 data (filled circles). Curves have been subjectively drawn to show the trend of the data. This figure is available in colour online at www.interscience.wiley.com/qj

that at high wind speed, the prongs of the sonic are being deformed, so the sound flight of time increases. This is just barely seen in the $u, v, w$ signals, because the sum of flight times enters the computations, but the temperature signal is strongly distorted as a result of it being derived from differences. Niels Mortensen made a wind-tunnel experiment with an R2 instrument, which was placed with its axis of symmetry oriented



DOI: 10.1002/qj

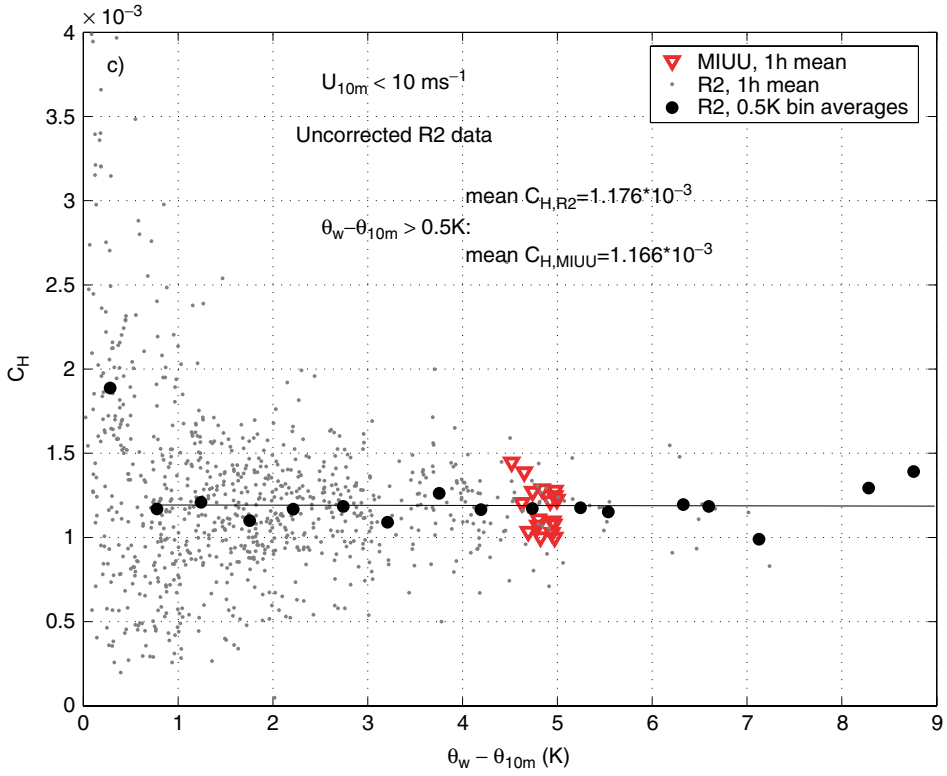


Figure 4. (*Continued*).

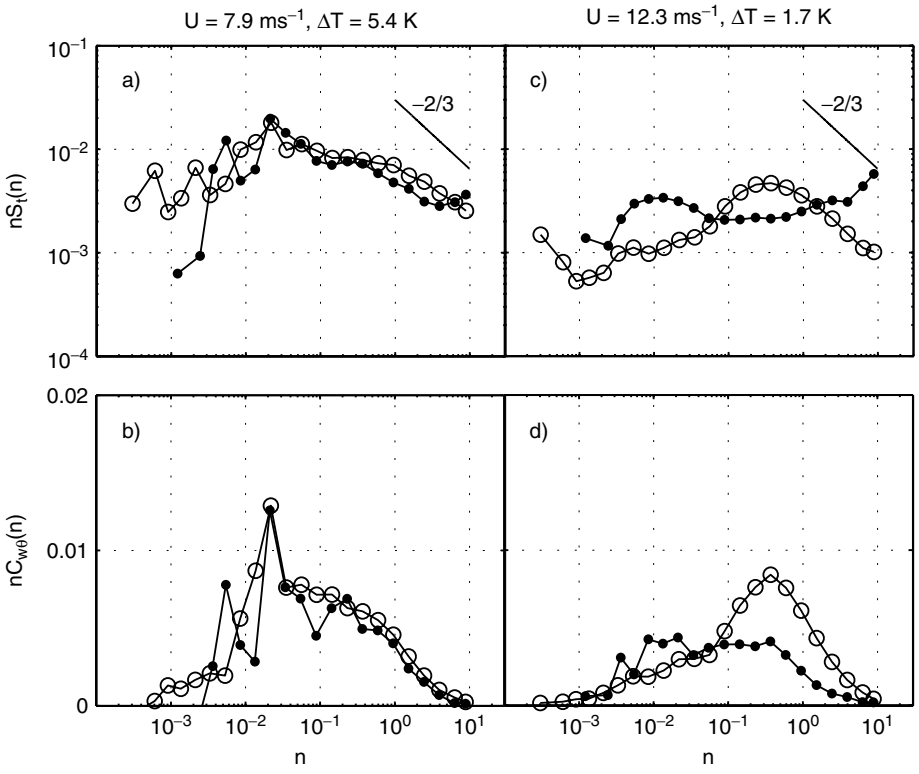


Figure 5. Comparison of simultaneous spectra from R3 (curves with dots) and the MIUU instrument (curves with open circles). Temperature spectra, (a) and (c) and corresponding $w\theta$ co-spectra, (b) and (d), with, for (a) and (b), a case with $U = 7.9$ m s$^{-1}$ and $\Delta\Theta = 5.4$ K and, (c) and (d), mean spectra from seven cases with $\overline{U} = 12.3$ m s$^{-1}$ and $\overline{\Delta\Theta} = 1.7$ K.



DOI: 10.1002/qj

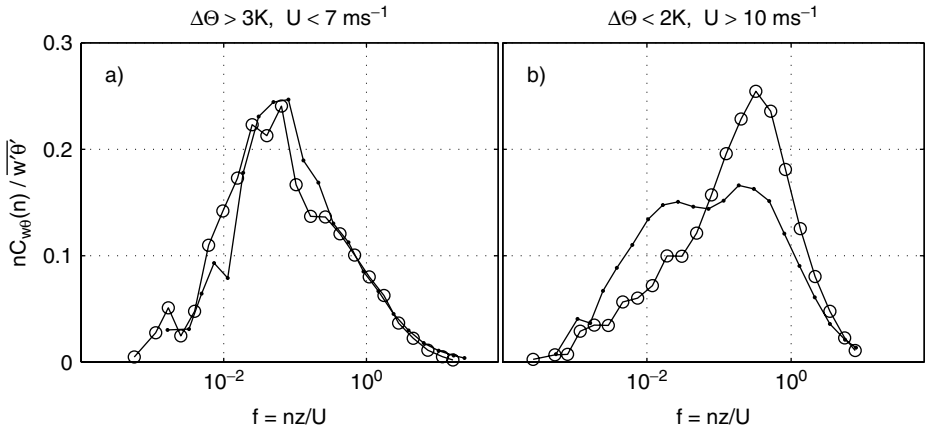


Figure 6. Mean R2 (dots) and MIUU (open circles) normalized $w\theta$ co-spectra for (a) a group of data with $U_{10} < 7$ m s$^{-1}$ and $\Delta\Theta > 3$ K ($N_{\text{sonic}} = 21$; $N_{\text{MIUU}} = 6$); and (b) a group of data with $U_{10} > 10$ m s$^{-1}$ and $\Delta\Theta < 2$ K ($N_{\text{sonic}} = 51$; $N_{\text{MIUU}} = 10$).

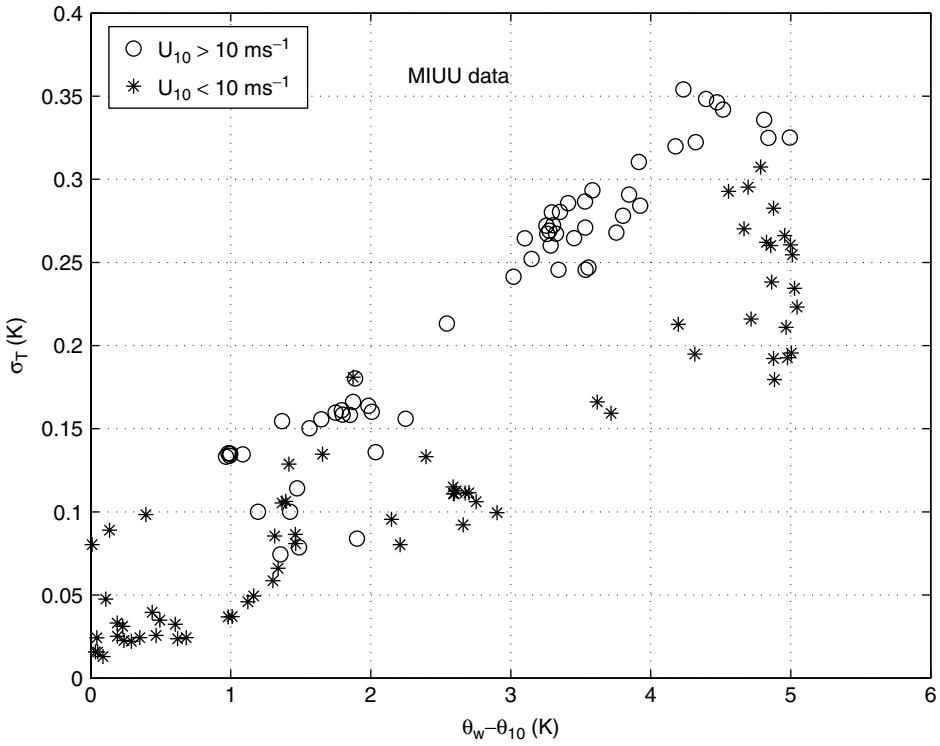


Figure 7. Temperature standard deviation $\sigma_T$, based on MIUU data, plotted against $\Delta\Theta$ for $U_{10} > 10$ m s$^{-1}$, circles, and for $U_{10} < 10$ m s$^{-1}$, stars.

horizontally. When he turned the instrument around its axis, he received a sinusoidal apparent temperature variation, which must have been related to a slight gravitational deformation of the sonic supporting prongs, an observation which appears to support the concept of mechanical deformation as the cause of the failure of the sonic instruments to record properly the heat flux in high wind.

The observations from Figure 4(a) and (b) that the sonics appear to record the heat flux truthfully in high winds provided the sea–air temperature difference is large enough (4–5 K) suggest that, if the temperature fluctuation level is high enough, this effect would outweigh the noise created by the deformation mechanism. Figure 7 shows the standard deviation of temperature fluctuation $\sigma_T$ plotted as a function of $\Delta\Theta$. For $U >$ 10 m s$^{-1}$ (open circles), there is a nearly linear relation between $\sigma_T$ and $\Delta\Theta$, and the criterion that $\Delta\Theta >$ c. 5 K for correct R2 fluxes in high-wind conditions could be equivalent to $\sigma_T >$ c.0.3 K. A reviewer expressed doubts about the results of Grelle and Lindroth (1996), in particular their Figure 6b, which shows measurements at 100 m height for a case with a wind speed of 12.2 m s$^{-1}$. The temperature curve obtained with the Pt sensor has a standard deviation of only 0.1–0.15 K (after removing an obvious trend), which is in line with the result that $\sigma_T$ should be at least double that for the R2 to truthfully record the heat flux.



DOI: 10.1002/qj

The conclusion from the above study is that R2 measurements of the sensible heat flux are acceptable for U $< 10$ m s$^{-1}$ for all temperature differences above c. 0.5 K and for wind speeds in the range 10–13 m s$^{-1}$ only for $\Delta\Theta > 4$–5 K, or perhaps $\sigma_T >$ c. 0.3 K. For the high-wind case, Equation (19) may be used as a rough correction. This factor, however, which amounts to as much as 1.6 for $U_{10} = 13$ m s$^{-1}$, i.e. a correction of 60%, must be considered with great caution. Therefore, in the analysis to follow in this paper, MIUU data are considered as the basis of the analysis and the R2 data will primarily be used to fill in the data space where needed.

## 5. Results

### 5.1. General trends of $C_H$ with wind speed and air-sea temperature difference

The MIUU-data plotted in Figure 4(a) and (b) show the variation of $C_H$ with $\Delta\Theta$ for the cases of $U > 12$ m s$^{-1}$ and $10 < U < 12$ m s$^{-1}$ respectively. The variation of $C_H$ with wind speed for the case of $\Delta\Theta > 3$ K is shown in Figure 8 (only MIUU data).

Equation (1) can be rewritten as a product of factors, which can be studied individually:

$$C_H = \overline{w'\theta'}/U_{10} \cdot (\Theta_w - \Theta_{10}) = (\overline{w'\theta'}/\sigma_w \cdot \sigma_T) \cdot (\sigma_T/-T_*) \cdot (\sigma_w/U_{10}) \cdot (-T_*/(\Theta_w - \Theta_{10}), \quad (20)$$

where the quantity in the first parentheses is $r_{w\theta}$, the correlation coefficient between $w$ and $\theta$.

Equation (20) has been applied to the data of $C_H$ against $\Delta\Theta$ for the case of $U_{10} > 10$ m s$^{-1}$. Each of the four factors on the right-hand side of Equation (20) were plotted individually against $\Delta\Theta$. Figure 9 shows the result for the last term, $-T_*/(\Theta_w - \Theta_{10})$. It is obvious that a dramatic change of the trend of the data appears at around $\Delta\Theta = 1.8$ K. The plots for the three other factors of Equation (20) show the respective parameter to vary smoothly with $\Delta\Theta$ (not shown here). Inspection of the data of Figure 9 reveals that for all points to the left of $\Delta\Theta = 1.8$ K, $-L > 150$ m and for all data to the right of that point, $-L < 150$ m. As will be shown in subsection 4.2, this $L$-value also marks a distinctive regime-change for $\phi_H$. Equation (7) shows that $-T_*/(\Theta_w - \Theta_{10})$ is a function of only two parameters (except the height $z$), $z_{0T}$ and $\psi_h$. This is an indication that the dramatic increase of $C_H$ for small values of $\Delta\Theta$ observed in Figure 4(a) and (b) is likely to partly be the result of processes related to the heat exchange at the surface, via $z_{0T}$, and partly to a change in the surface-layer turbulent heat exchange regime, through $\phi_H$ and its integral $\psi_h$. This point will be further explored in forthcoming subsections.

With the aid of Equation (11), the data will later be converted to $C_{HN}$. But that will require information about $z_{0T}$, which will be evaluated from Equation (7). This quantity, in turn, requires information about $\phi_h(z/L)$, which will be discussed in next subsection.

### 5.2. Dimensionless temperature profiles, $\phi_H(z/L)$

Evaluation of $\phi_H$, Equation (7), requires information about the vertical gradient of potential temperature. Mean

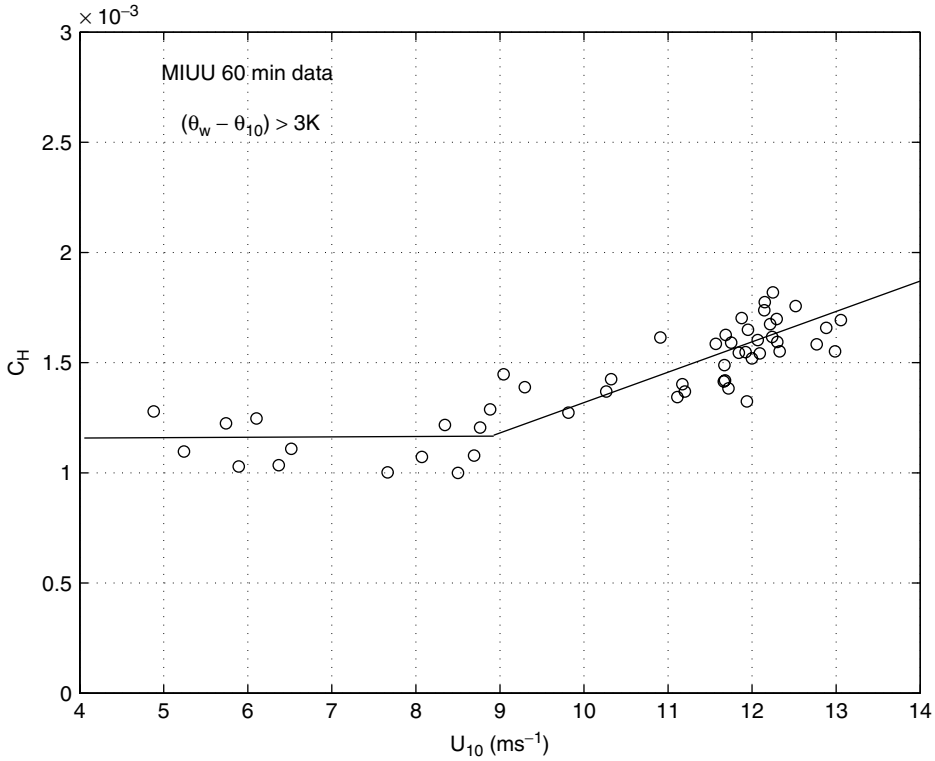


Figure 8. $C_H$ (60-minute mean values) plotted against $U_{10}$ for the case $\Delta\Theta > 3$ K. Only data with heat flux obtained with the MIUU instrument.



DOI: 10.1002/qj

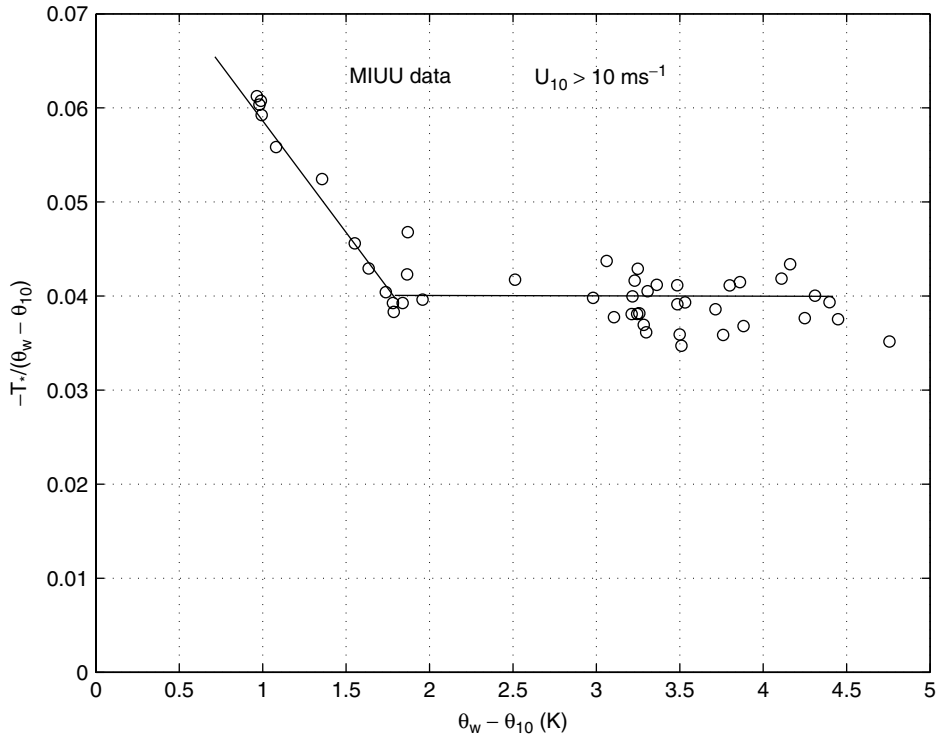


Figure 9. The quantity $|T_*|/(\Theta_w - \Theta_{10})$ plotted against $\Delta\Theta$, for $U_{10} > 10$ m s$^{-1}$. All data points are based on measurements with the MIUU instrument.

temperature is measured at five levels on the tower, 7, 12, 14, 20 and 29 m. These are nominal heights, the actual heights being dependent on the actual mean sea level. Plots of $T_* = -\overline{w'\theta'}/u_*$ against $\Theta_{i+1} - \Theta_i$ for each of the four consecutive height intervals (not shown here) enabled drawing best fit lines from which it was possible to infer $x$-intercepts for zero heat flux. The intercepts were respectively +0.01 K, −0.02 K, 0.00 K and −0.02 K for, respectively, the 12–7 m, 14–12 m, 20–14 m and 29–20 m difference, which is well within the range expected from the laboratory calibrations. The encountered temperature differences are, however, very small: less than 0.05 K for the 7–12 m and 12–14 m intervals and less than 0.1 K for the two higher intervals. Inspection of individual temperature profiles revealed that smooth lines could be drawn as a fit to most profiles for the height interval 12–29 m, whereas in many cases, the 7 m point deviated systematically from the general trend for the other heights. Because of this, the potential temperature gradient at 10 m was simply taken as $(\Theta_{12} - \Theta_7)/5$, whereas the corresponding gradients for 16 and 26 m were obtained from differentiation of a best-fit second-order polynomial in log–linear representation, based on data from 12, 14, 20 and 29 m. All temperatures were first corrected for the small zero offsets described above.

In Figure 10, $\phi_H$ at 10 m is plotted as a function of $z/L$. The figure includes MIUU data as well as R2 data, in accordance with the notations in the graph. The R2 data have been chosen according to the criterion $\overline{w'\theta'} > 0.02$ m s$^{-1}$ K and, for cases with wind speeds >10 m s$^{-1}$, have been corrected with Equation (19). It is clear that most of the data follow Högström's (1988) equation reasonably well:

$$\phi_H = 0.95(1 - 11.6z/L)^{-1/2}. \tag{21}$$

However, almost all data with $-L > 150$ m deviate strongly downwards. As discussed in detail in the companion paper (Smedman *et al.*, 2007), these data represent a turbulence regime which we have chosen to term 'the unstable very close to neutral regime', or 'the UVCN regime' and which turns out also to occur during similar conditions over land. Thus, analysis of MIUU data from a surface-layer experiment over land shows that the strong drop in $\phi_H$ is equally evident at 6.3, 3.1 and 1.6 m above the surface during these conditions.

Figure 11 shows $\phi_H$ at 17 and 26 m (symbols according to legend). Here, the same criterion on R2 data has been employed as in the case of Figure 10. The data points are slightly above the curve represented by Equation (21), but the trend follows the curve closely. We notice that a very small systematic offset in the temperature differences, well within the measurement accuracy, is enough to cause this offset, so we conclude that Equation (21) is indeed valid at 17 and 26 m. Note that there are no systematic excursions downward of data for $-L > 150$ m. As discussed in the companion paper, this result is in agreement with the expectations from the theory for the new regime.

Thus, also considering the result of Figure 11, we conclude that MO-theory is invalid for cases with $-L >$



DOI: 10.1002/qj

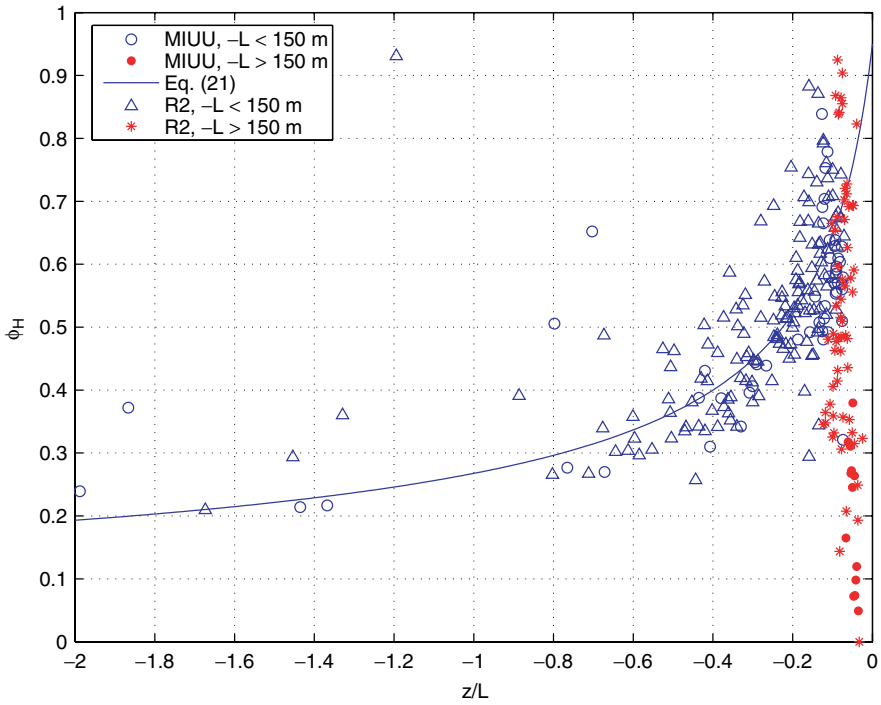


Figure 10. Dimensionless temperature gradient $\phi_H$ plotted against $z/L$ at 10 m. The plot contains both data obtained with the MIUU instrument and data obtained with the R2 (corrected with Equation (19) for winds above 10 m s$^{-1}$), see insert legend. Filled circles and stars are data with $-L > 150$ m. The curve is from Högström (1988). This figure is available in colour online at www.interscience.wiley.com/qj

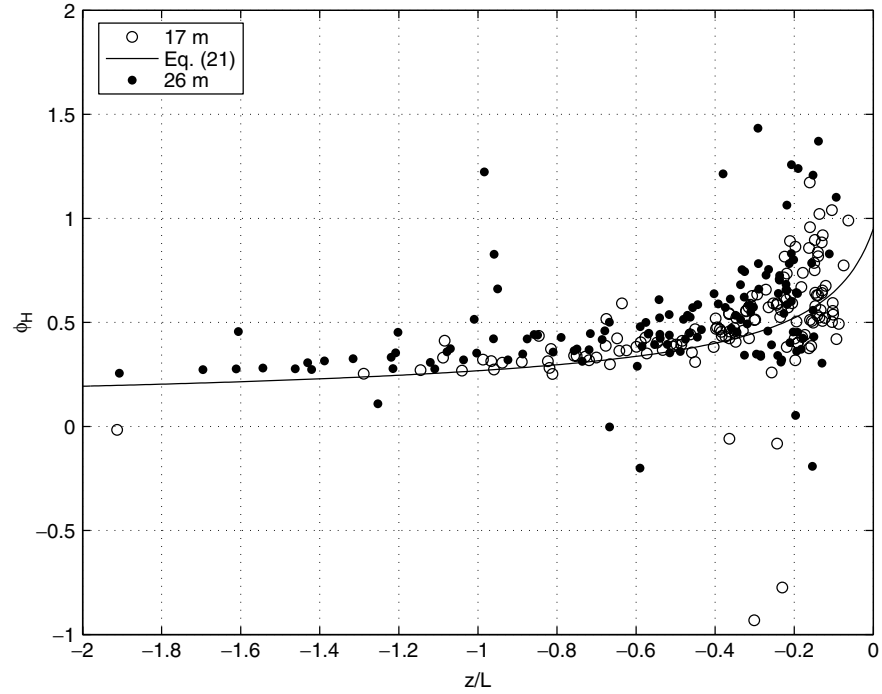


Figure 11. Dimensionless temperature gradient $\phi_H$ at 17 m (open circles) and at 26 m (filled circles) plotted against $z/L$. The curve is obtained from Högström (1988).

150 m from a height of around 12–15 m down to the surface. It implies that for those cases, it is impossible to evaluate $\psi_h$ from Equation (9). Formally, we set $\psi_h = 0$ and evaluate an '*apparent*' $z_{0T}$-value from Equation (11), assuming $C_H = C_{HN}$, where $C_H$ is evaluated from Equation (1). This approach is considered reasonable for the high-wind cases which comprise this group of data.

### 5.3. Evaluation of $C_{HN}$

Figure 12 shows $C_{HN}$, evaluated with Equation (11) and plotted against $U_{10}$. The open circles are individual hourly mean values for $C_{HN}$, obtained with the MIUU instrument for the cases with $-L < 150$ m. The filled circles are 1 m s$^{-1}$ bin averages based on R2 data corrected with



DOI: 10.1002/qj

Equation (19). The remaining are MIUU data for cases with $-L > 150$ m. With reference to the legend, these data are seen to order according to the magnitude of the sea surface – air temperature difference, with large $C_{HN}$ values for small temperature differences. The trend of the R2-bin average data points (filled circles) in Figure 12 differs slightly from that of the corresponding MIUU data for $U_{10} < 9$ m s$^{-1}$. This may be a reflection of the fact that the MIUU data represent only a time period of a few days, which may not have the same mix of wave age conditions as the much more extensive R2 dataset. For the data with $-L > 150$ m, highly tentative lines have been fitted by eye. The two horizontal lines are also tentative fits to the MIUU data (lower line) and R2 data (upper line) respectively. For the MIUU data with $-L < 150$ m and $U_{10} > 8$ m s$^{-1}$, another tentative line has been fitted. The R2 data are seen to follow the trend of this line up to about 11.5 m s$^{-1}$ and to increase more rapidly for higher wind speeds. As the individual R2 data are very scattered for high winds (not shown), no attempt was made to make a subdivision according to temperature difference. Note that $U_{10}$ in Figure 12 is measured wind speed. Often $C_{HN}$ is plotted against 10 m wind speed 'reduced to neutral', but since previous studies of our group have shown (Smedman *et al.*, 2003) that the shape of the neutral wind profile is strongly wave-age-dependent, we have chosen not to make such a reduction here.

In Figure 13 the effect of the $\phi_m$-parametrization on $C_{HN}$ is evaluated on the MIUU data. The open circles represent the basic case, with $\phi_m$ derived with Equations (12)–(16), in accordance with prevailing wave age and $z/L$ for each individual case. The filled circles represent the situation when $\phi_m$ is always derived with the expression for growing sea, Equation (12), which is, in practice, equivalent to the procedure used in the COARE3.0 algorithm. The wave-age effect at 5–6 m s$^{-1}$ amounts to decreasing $C_{HN}$ by about 20%, the corresponding effect at 11 m s$^{-1}$ being of the order 5%.

Figure 14 illustrates the combined effect of $\phi_m$ and $z_0$ on $C_{HN}$. The open circles represent the basic case in which $z_0$ was evaluated from Equation (6), with $\psi_m$ being derived from Equations (12)–(16). The filled circles represent the same cases, but $z_0$ was taken from the COARE3.0 algorithm (Fairall *et al.*, 2003), which amounts to applying the Charnock relation $z_0 = \alpha u_*^2/g$, 'where $\alpha$ increases linearly from 0.011 at $U_{10} =$ 10 m s$^{-1}$ to 0.018 at $U_{10} = 18$ m s$^{-1}$, and remains constant for lack of better information beyond this wind speed'. It is clear from Figure 14 that for $U_{10} <$ 10 m s$^{-1}$, the present data gives systematically lower $C_{HN}$ values, $0.88 \times 10^{-3}$ compared to the COARE3.0 parametrization, which gives $1.11 \times 10^{-3}$. For $U_{10} >$ 10 m s$^{-1}$, the two $z_0$ parametrizations give very similar results, other factors unchanged.

Fairall *et al.* (2003) give the COARE3.0 expression for the roughness length for heat:

$$z_{0T} = z_{0q} = \min(1.1 \times 10^{-4}, 5.5 \times 10^{-5} R_r^{-0.6}), \quad (22)$$

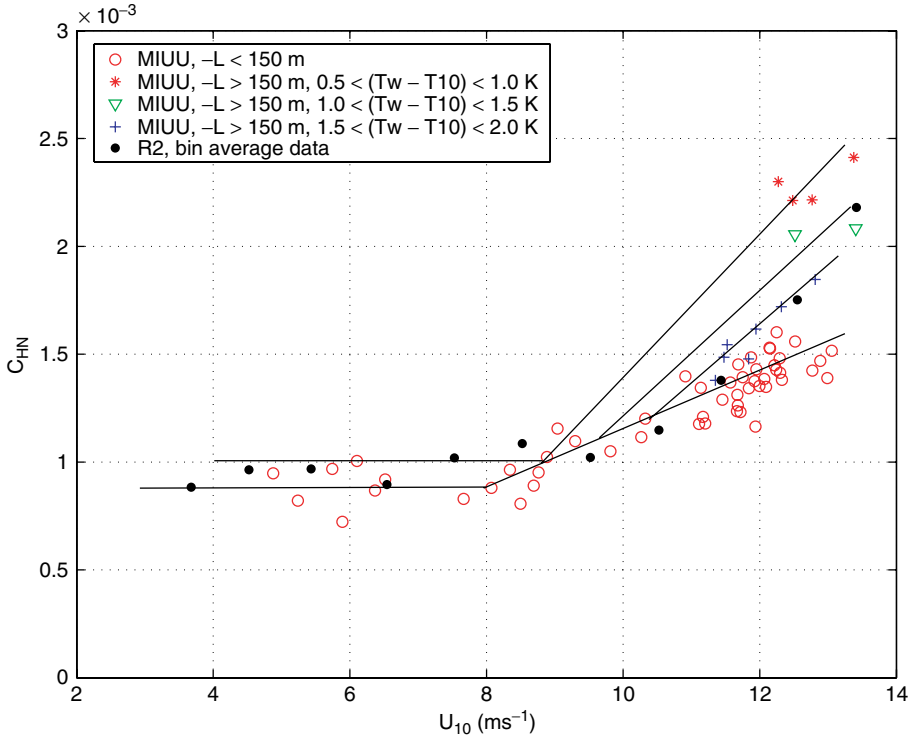


Figure 12. $C_{HN}$ plotted against wind speed at 10 m. Black circles are bin averages of $C_{HN}$ based on R2 data corrected with Equation (19); remaining data are 60 min MIUU data of $C_{HN}$. All lines are tentative fits (see text for details). This figure is available in colour online at www.interscience.wiley.com/qj



DOI: 10.1002/qj

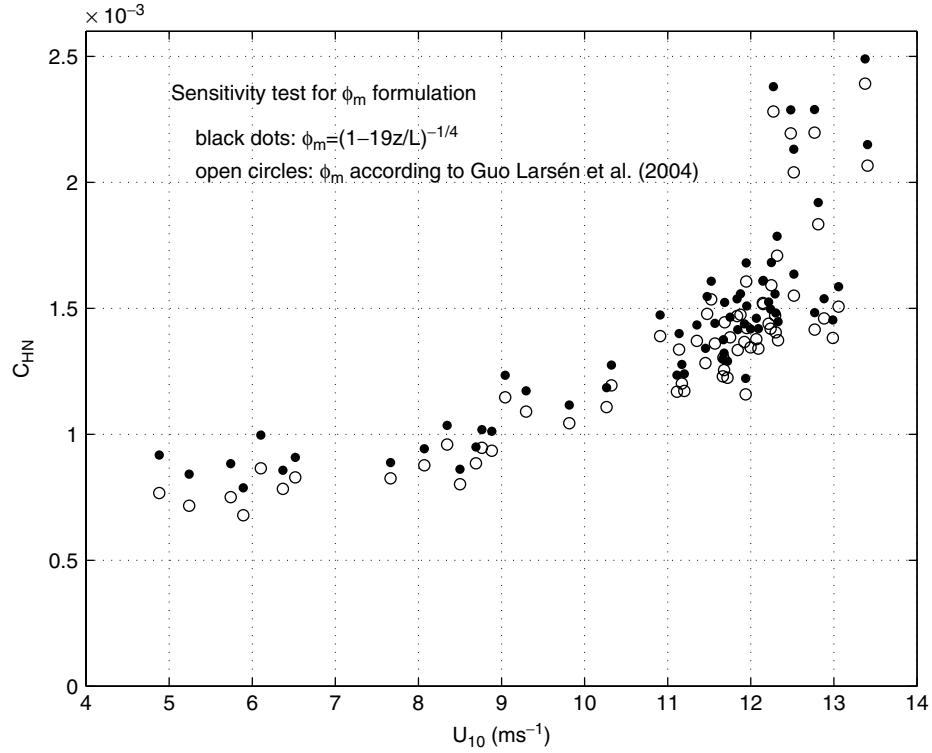


Figure 13. $C_{\mathrm{HN}}$ sensitivity test for the MIUU data regarding formulation for dimensionless wind profile $\phi_m$ (see insert legend and text for details).

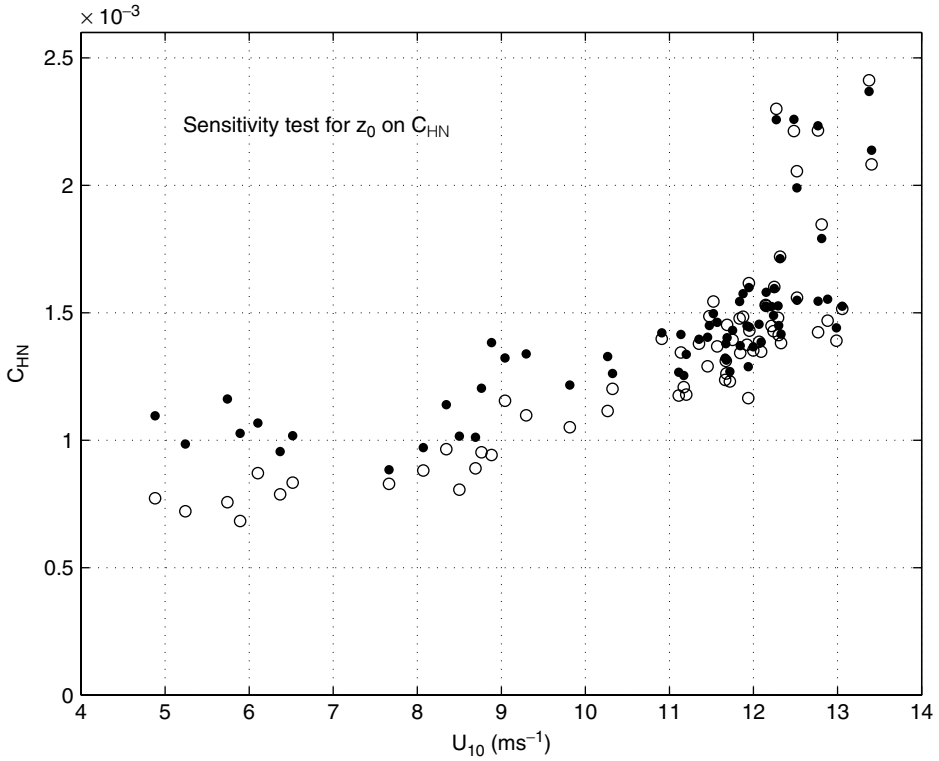


Figure 14. $C_{\mathrm{HN}}$ sensitivity test for the MIUU data regarding formulation of momentum roughness length $z_0$. Open circles, basic parametrization; closed circles, $z_0$ formulation according to COARE 3.0.

where $R_{\mathrm{r}} = u_* z_0/\nu$ is the roughness Reynolds number. Figure 15 presents two versions of $C_{\mathrm{HN}}$: (i) the basic case, represented by open circles, for which $z_{0T}$ is obtained with Equation (7) from measurements of $\Theta_{\mathrm{w}} - \Theta_{10}$ and $T_*$ and with $\psi_h$ being derived with Equations (9) and (21), and (ii) $z_{0T}$ obtained with Equation (22), filled



DOI: 10.1002/qj

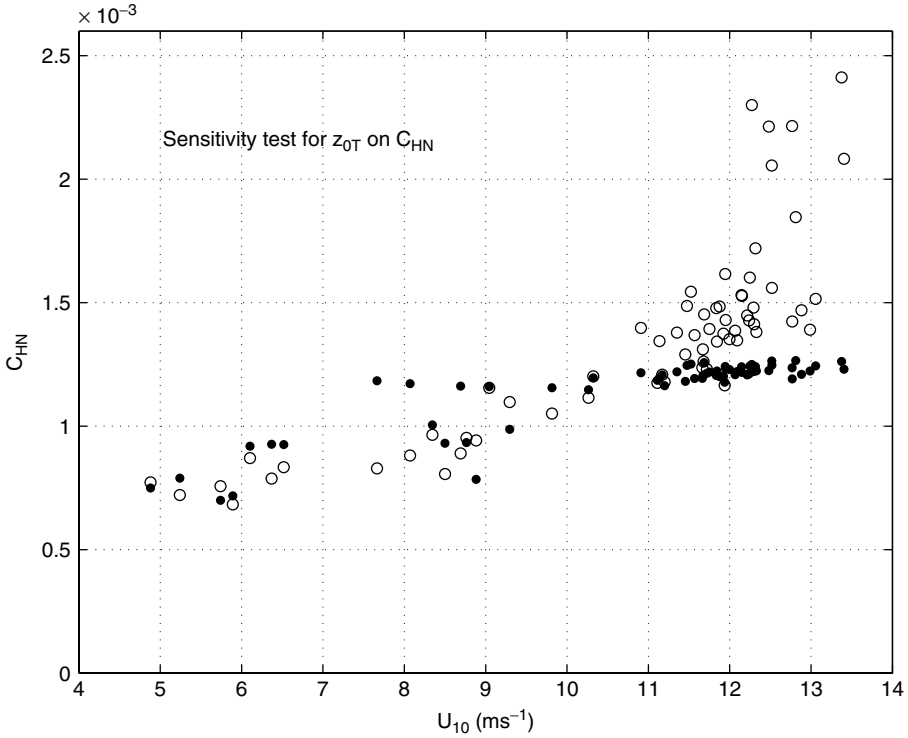


Figure 15. $C_{\mathrm{HN}}$ sensitivity test regarding formulation of temperature roughness length $z_{0T}$. Open circles, basic parametrization; closed circles, $z_{0T}$ formulation according to COARE 3.0.

circles. For the two cases (i) and (ii), $z_0$ is obtained in the same way, i.e. with Equations (12)–(16). Below about 11 m s$^{-1}$ the two datasets do not differ in a systematic way, but for higher wind speed, the difference is striking: whereas the open circles continue to increase rapidly with wind speed, the filled circles remain nearly constant. This means that for wind above 10 or 11 m s$^{-1}$, $z_{0T}$ is very different in our case compared to the COARE3.0 parametrization, Equation (22), and that this has decisive influence on $C_{\mathrm{HN}}$.

Fairall *et al.* (2003) argue that a modified 'surface-renewal-relation' adequately describes their data for $U_{10} < 18$ m s$^{-1}$:

$$R_q = R_{\mathrm{r}} \exp(3.4 - 3.5 R_{\mathrm{r}}^{1/4}), \tag{23}$$

where

$$R_q = u_* z_{0q}/\nu = R_t = u_* z_{0T}/\nu. \tag{24}$$

Figure 16 shows, in a log–log representation, $R_t$ against $R_{\mathrm{r}}$. Open circles are MIUU data for $U_{10} < 10$ m s$^{-1}$, open stars MIUU data with $U_{10} > 10$ m s$^{-1}$ and $-L < 150$ m, and 'black' stars MIUU data with $-L > 150$ m; black circles are R2 bin-average data for $U_{10} < 10$ m s$^{-1}$ and triangles R2 bin-average data (corrected with Equation (19)) for $U_{10} > 10$ m s$^{-1}$. It is clear that all data with $U_{10} < 10$ m s$^{-1}$ follow Equation (23) in the mean, but that data with $U_{10} > 10$ m s$^{-1}$ are found to set off into a regime roughly characterized by $R_t = R_r$, or equivalently, $z_{0T} = z_0$. Some of the stars, i.e. the cases with $-L > 150$ m are even higher, but for those cases we know that MO-theory is not valid, which makes interpretation of '$z_{0T}$' difficult; see next section for a discussion.

Figure 17 shows, for R2 data, $C_{\mathrm{HN}}$ against $U_{10}$ for wind speeds in the range $3 < U_{10} < 10$ m s$^{-1}$, divided according to wave age, $c_{\mathrm{p}}/U_{10}$. In this wind speed range, $C_{\mathrm{HN}}$ is found to be approximately invariant with wind speed but systematically varying with wave age, with the following mean values: for growing sea ($c_{\mathrm{p}}/U_{10} < 0.8$), $C_{\mathrm{HN}} = 1.09 \times 10^{-3}$; for mature sea ($0.8 < c_{\mathrm{p}}/U_{10} < 1.2$) $C_{\mathrm{HN}} = 1.01 \times 10^{-3}$ and for swell ($c_{\mathrm{p}}/U_{10} > 1.2$) $C_{\mathrm{HN}} = 0.91 \times 10^{-3}$. Most of the wave-age-dependent variation seen in this figure is related to the parametrization of $\phi_m$, Equations (12)–(16).

### 5.4. Test of the COARE3.0 algorithm on the MIUU data

The COARE3.0 algorithm (Fairall *et al.*, 2003) has been applied on the MIUU data used in the present study to calculate the sensible heat flux, which is then compared to corresponding measured fluxes. It amounts to calculating $C_{\mathrm{H}}$ with Equation (10), with values of $z_0, z_{0T}, \phi_m$ and $\phi_H$ derived with the corresponding expressions given in Fairall *et al.* (2003) and finally calculating $\overline{w'\theta'}$ with Equation (1). The result is presented in Figure 18. For the 49 cases with $U_{10} > 10$ m s$^{-1}$ the mean measured flux is 0.0574 m s$^{-1}$ K and the corresponding mean COARE3.0-calculated value is 0.0410 m s$^{-1}$ K, i.e. the COARE3.0 algorithm underestimates the sensible heat flux for this data set by as much as 40%, or 0.0164 m s$^{-1}$ K. For $U_{10} < 10$ m s$^{-1}$ the COARE3.0 algorithm tends to overestimate the heat flux slightly.



DOI: 10.1002/qj

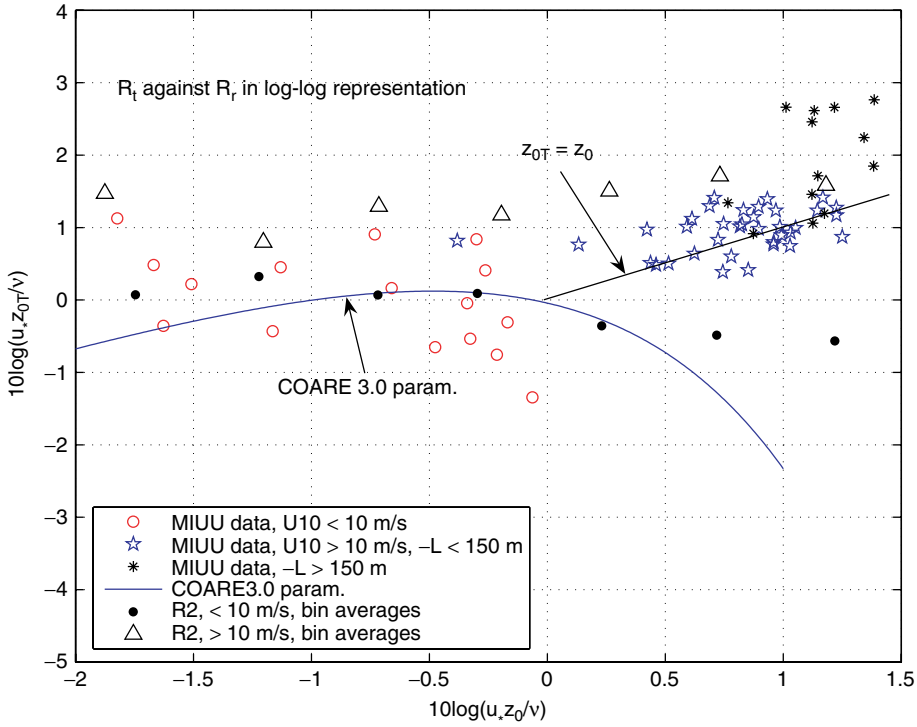


Figure 16. Logarithm of roughness Reynolds number for heat $R_t = u_* z_{0T}/\nu$ plotted against the corresponding logarithm of roughness Reynolds number for momentum $R_r = u_* z_0/\nu$. Notations: see insert legend and text. This figure is available in colour online at www.interscience.wiley.com/qj

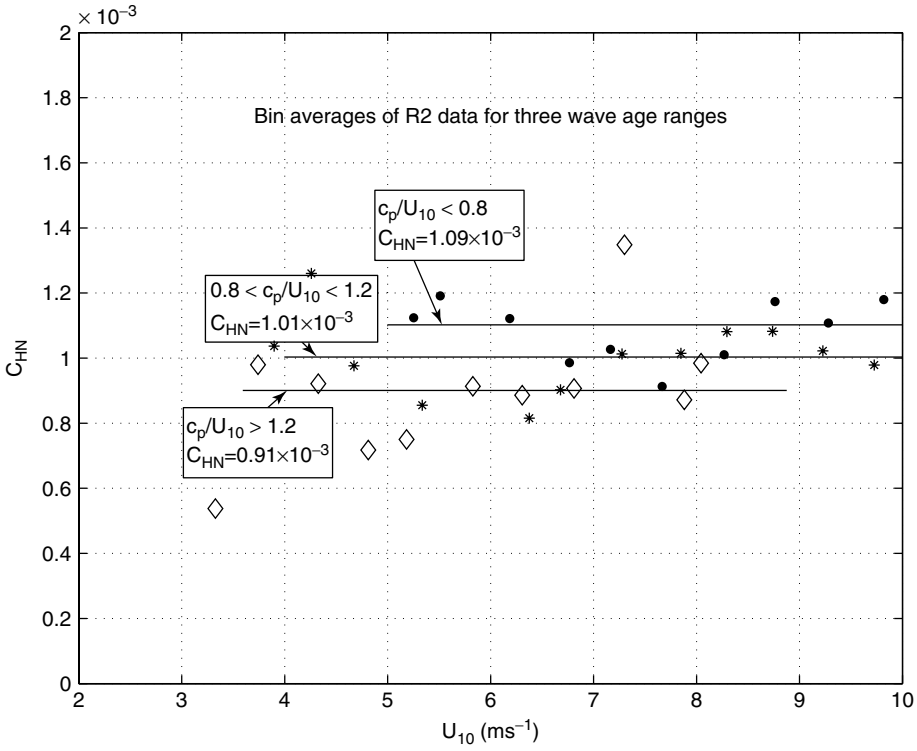


Figure 17. Bin average R2 data for $C_{HN}$ plotted against wind speed and divided according to wave age, for the wind speed range $3 < U_{10} < 10$ m s$^{-1}$. Legend: filled circles, $c_p/U_{10} < 0.8$; stars: $0.8 < c_p/U_{10} < 1.2$; diamonds, $c_p/U_{10} > 1.2$.

## 6. Discussion and comparison with other data

The above results have clearly demonstrated that $C_{HN}$ increases rapidly with wind speed for $U_{10} > 8$ m s$^{-1}$ (Figure 12) and that this is intimately linked to a strong increase in $z_{0T}$ for $U_{10} > 10$ m s$^{-1}$ compared to what is expected from surface-renewal theory, Liu *et al.* (1979) and the modified form in Fairall *et al.* (2003).



DOI: 10.1002/qj

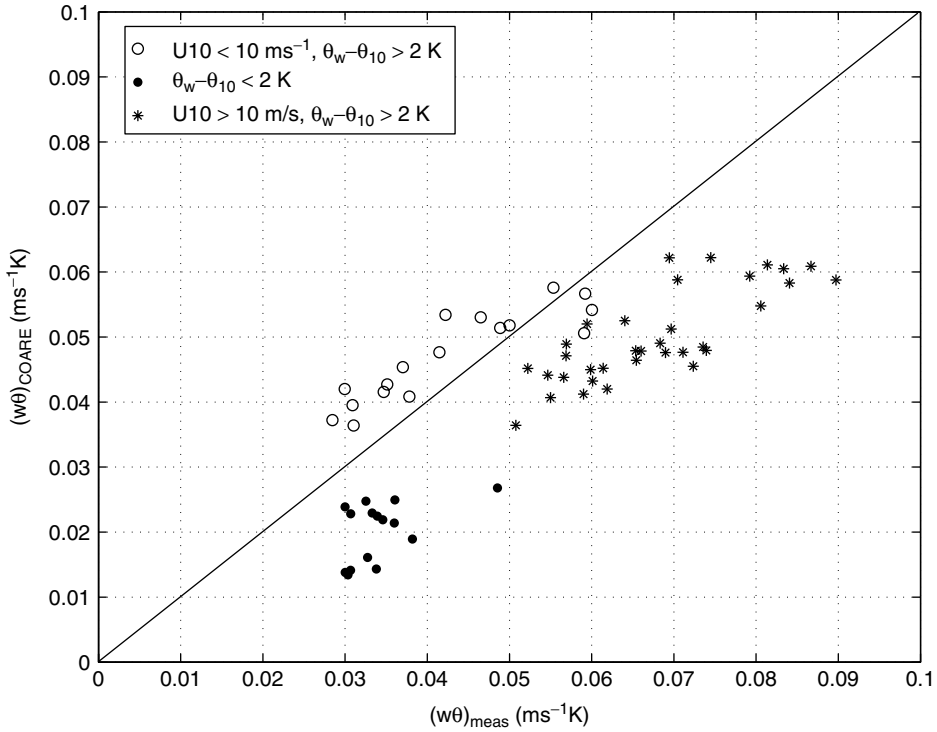


Figure 18. Test of the COARE3.0 algorithm for sensible heat flux against measured MIUU data.

Table I gives a schematic overview of some of the most well-known previous published results for $C_{HN}$. In the last column of the table an indication is given concerning occurrence/non-occurrence of a 'clear' or 'possible' velocity trend in the published results. Note (fifth column) that most previous studies have a criterion for a minimum sea surface – air temperature difference for acceptance of data, and that Figure 4(a) shows that most of the rise in $C_H$ appears for $\Delta\Theta < 2$ K. Thus, one cannot rule out the possibility that most of the dramatic rise of $C_{HN}$ that we observe may have escaped observation in some of the previous studies.

Among the studies listed in Table I, there is one which shows a very clear rise of $C_{HN}$ with wind speed: Francey and Garratt (1979). The measurements were taken within the Air-Mass Transformation Experiment (AMTEX) during cold air outbreaks over the East China Sea. The measurements were performed with the CSIRO FLUXATRON instrumentation (vertical-axis Gill propeller for vertical velocity plus six-cup anemometer for horizontal velocity plus bead thermistor) on a tower situated near the shore of a small island with a coral reef extending 200 m from the shore. Calculations by the authors indicate that the effects of the reef on $C_{HN}$ were expected to be small. The trend of $C_{HN}$ plotted against $U_{10}$ is very similar to that of the present study.

Another study which indicates that traditional parametrizations, which take $C_{HN}$ to be essentially constant, give systematically low heat flux values for strong winds is listed on the last line of Table I. Brunke *et al.* (2003) evaluated 12 flux algorithms against data from 12 experiments and found that all schemes strongly underestimated the sensible heat fluxes from CATCH, which is an experiment with high frequency of strong winds. Reanalysis of the CATCH data by Weill *et al.* (2003), which attempts to take into account effects of flow distortion around the ship, lowers the $C_{HN}$ data slightly but still indicates possible increase in high winds.

The analyses of the measurements in COARE reported in Clayson *et al.* (1996) and in Chang and Grossman (1999) clearly show that the COARE model, which has essentially constant $C_{HN}$, systematically underestimates the sensible heat flux in the range $8 < U_{10} < 12$ m s$^{-1}$.

The study of Pedreros *et al.* (2003) is particularly interesting. It reports simultaneous measurements with Solent sonic anemometers of $C_{HN}$ on a ship and on an ASIS (Air–Sea Interaction Spar) buoy. Eddy correlation measurements give $C_{HN}$ data that mutually agree and which are found to be virtually constant for $2 < U_{10} < 17$ m s$^{-1}$. But corresponding $C_{HN}$ data derived with the inertial-dissipation method (IDM) from the sonic onboard the ship show a clear increase with wind speed. Although IDM results must be treated with great caution (see e.g. Sjöblom and Smedman, 2003b), as noted in section 4 and discussed in some detail below, sonic R2 data for the flux of sensible heat are probably erroneous for winds above c. 10 m s$^{-1}$ (except for cases with $\Delta\Theta > 4$–5 K).

It is notable that many studies have high values for near-neutral conditions. This is clearly seen in Wu's (1992) reanalysis of the data from Friehe and Schmitt (1976) and from Smith (1980). In Wu's Figure 3, $C_H$ is plotted against $U_{10}\Delta T$, showing very high values close to $U_{10}\Delta T = 0$.



DOI: 10.1002/qj

Table I. Results from previous studies of $C_{HN}$ reported in the open literature.

| Reference | Dataset | Instrumentation | Method | Criter. for $\Delta\Theta$ (K) | $U$-range ($ms^{-1}$) | $C_{HN}U$-trend |
|---|---|---|---|---|---|---|
| Friehe and Schmitt (1976) | Several old data | various | EC | no info | no info | possible |
| Francey and Garratt (1979) | AMTEX | Fluxatron | EC | >4.5 | 5–13 | clear |
| Smith (1980) | BIO tower | Thrust anemometer +thermistor | EC | >1.0 | 6–21 | possible |
| Large and Pond (1982) | BIO-tower + ships | Twin prop.vane +thermistor | IDM | >1.0 | 4–17 | weak |
| DeCosmo *et al*. (1996) | North Sea tower (HEXOS) | Sonic + twin prop.-vane +thermistor | EC | >1.5 | 6–20 | no |
| Clayson *et al*. (1996) | COARE + TIWE + ASTEX | Solent R2 | EC | no info | <12 | for $U > 8$ $ms^{-1}$ |
| Chang and Grassman (1999) | COARE | Solent R2 | EC | no info | < 12 | for $U > 8$ $ms^{-1}$ |
| Oost *et al*. (2000) | North Sea tower | Solent R2A +thermocouple | EC | >0.8 | 2–18 | possible |
| Pedreros *et al*. (2003) | FETCH: ship+ ASIS buoy | Ship: R3HS; ASIS: R2A | EC+ IDM | >2.0 | 2–17 | In IDM |
| Brunke *et al*. (2003) + Eymard *et al*. (1999) | 12 exper, 12 algo-rithms; spec.: CATCH | Solent R2 | IDM | >1.5 | 5–30 | possible in CATCH |

Method: EC = eddy-correlation method; IDM = inertial-dissipation method. – Notes: the Friehe and Schmitt (1976) data are for $C_H$, all others are for $C_{HN}$. Brunke *et al*. (2003) + Eymard *et al*. (1999): the results refer to the model predictions for the flux of sensible heat compared to the corresponding measurements during CATCH (cf. also Weill *et al*., 2003).

Oost *et al*. (2000) measured the sensible heat flux with a combination of a sonic R2A for vertical velocity and a thermocouple for temperature. Although the scatter is large in their Figure 6, it shows clearly that their data for the case $L < 0$ and $T_{air} < T_w$ increase with wind speed, their mean value for $C_{HN}$ at 5 m $s^{-1}$ being about $0.8 \times 10^{-3}$ and for 15 m $s^{-1}$about $1.8 \times 10^{-3}$.

The study of Large and Pond (1982) shows a weak increase of $C_{HN}$ with wind speed, but the scatter is very large, and uncertainties related to the ID method must be considered.

The HEXOS results for $C_{HN}$ (DeCosmo *et al*., 1996) show no tendency for increase with wind speed. The data are based on measurements with several instruments for vertical velocity and separate instruments for temperature. As the authors exclude all data with $\Delta\Theta < 1.5$ K, there is of course the possibility that high values may have been deleted by mistake. It is also worth noticing that the study of Oost *et al*. (2000), which indeed indicates wind speed variation for $C_{HN}$, was obtained from the same platform.

The results from the HEXOS study was used by Fairall *et al*. (2003), together with data from 'six NOAA cruises, ...preliminary results from two other ETL [NOAA/Environmental Technology Laboratory] programs, and other published measurements from high wind regions, to extend the applicability [of the new COARE algorithm] to 20 m $s^{-1}$'. Although details are not given in Fairall *et al*. (2003) about all these cruises, it is stated that EC (eddy-correlation) measurements were done with the same instrumentation, which in the case of the sensible heat flux means that it was derived solely from Solent sonic data (Fairall *et al*.,1997). Considering the problems encountered with this instrument for $U_{10} > 10$ m $s^{-1}$, section 4, it is possible that for those high-wind cases, the sensible heat flux estimates may be erroneous.

Fairall *et al*. (2003) find that $z_{0T}$ equals $z_{0q}$, which appears to follow predictions from surface-renewal theory (Liu *et al*., 1979) for all conditions. As discussed in the previous section, our results clearly indicate a regime shift around $U_{10} = 10$ m $s^{-1}$, Figure 16, with $z_{0T}$ increasing much more rapidly with $R_r$ than predicted from surface-renewal theory. The exact mechanism for this is not known, but already Donelan (1990) speculated that increase of wave slope leads to an increase of surface area and possible disruption of the surface microlayer, which would act to increase the total heat flux. It is clear from recent air–sea tank experiments and theoretical studies (several presentations at 37th International Liège Colloquium on Ocean Dynamics, 2–6 May 2005, 'Gas Transfer at Water Surfaces'; to be published in *J. Marine Systems*) that air–sea transfer is highly intermittent and that wave breaking plays a crucial role, which includes both 'ordinary' large-scale breaking and 'microscale breaking', which starts to occur at wind speeds as low as 4–5 m $s^{-1}$ and which may be widespread. A further possible link to near-surface atmospheric processes during strong downdraughts is discussed in the companion paper (Smedman *et al*., 2007).



DOI: 10.1002/qj

Because of its limited geographical extent, the Baltic Sea is likely to have a wave climate that differs from that typical of the deep sea, and this, in turn, is likely to influence the statistical distribution of $z_0$. But as illustrated in the previous section (Figure 14), this is likely to primarily influence the level of $C_{HN}$ for $U_{10} < 10$ m s$^{-1}$. The strong rise of $C_{HN}$ for $U_{10} > 10$ m s$^{-1}$ (Figure 12) occurs in a wave regime which has been documented at Östergarnsholm to be very similar to that observed over the deep sea (Smedman *et al*., 2003). Thus, it appears highly unlikely that the observed increase of $C_{HN}$ with wind speed above 10 m s$^{-1}$ is due to wave conditions that are peculiar for the Baltic Sea at large or the Östergarnsholm site in particular.

## 7. Conclusions

The present analysis of the Östergarnsholm data is primarily based on a limited set of measurements with the very accurate MIUU instrument, but with additional information from an extensive set of measurements with Solent sonic R2, which were, however, subject to a strongly wind speed dependent correction of the sensible heat flux for winds above 10 m s$^{-1}$. The error in the sonic-derived heat flux was also shown to depend on the air–sea temperature difference (or possibly more fundamentally, on the temperature standard deviation), MIUU and sonic fluxes being equal for $\Delta\Theta > 4$–5 K.

It was inferred that for conditions when unstable and near-neutral conditions prevail, measurements of the sea surface – air temperature difference were accurate to within 0.1 K. This means that data for a range of relatively small temperature differences (0.5–1.5 K) which have often been rejected in previous studies could be retained. It was observed that a rapid increase of $C_H$ and $C_{HN}$ occurs in that range.

It was found that in the range $4 < U_{10} < 8$ m s$^{-1}$, $C_{HN}$ is lower than most previous studies suggest, and it was demonstrated that this was largely due to the effect of small values for $z_0$, caused by frequent occurrence of wind-following swell and mixed-sea conditions in the Baltic Sea. This may be different in typical deep-sea conditions. For higher wind speed, $C_{HN}$ was observed to increase rapidly with $U_{10}$. During those conditions, the wave field at the site is known to have characteristics very similar to those in deep-sea conditions. In a previous analysis of data from Östergarnsholm, it was speculated that observed high $C_{HN}$ values could be due to spray. Calculations with the Andreas (2004) spray model by Sahlée *et al*. (2007) showed, however, conclusively that for wind speeds less than 14 m s$^{-1}$, the spray effect on the sensible heat flux is expected to be less than 10%. The high $C_{HN}$ values must instead be due to dynamic effects.

It was demonstrated that when the Obukhov length $L$ attains large enough negative value $\approx -150$ m, a regime with very specific characteristics ensues, called the unstable very close to neutral regime, or the UVCN regime. This regime is dominated by surface-layer scale eddies, which cause MO-relations for the exchange of sensible heat to break down. The characteristics of this surface-layer regime are treated in detail in the companion paper, Smedman *et al*. (2007).

The rise of $C_{HN}$ with wind speed was shown to be closely related to a corresponding increase of $z_{0T}$ with roughness Reynolds number for winds above 10 m s$^{-1}$. This means that during those conditions, surface renewal theory for heat is no longer valid. It is suggested that this, in turn, is a result of increasing importance of wave-breaking with increasing wind and with a possible link to processes in near-surface atmospheric layers in the UVCN regime.

## Acknowledgements

This work was funded by The Swedish Research Council, grant no 621-2002-5348. We wish to thank Dr Hans Bergström and other colleagues at MIUU who are responsible for the measurements at Östergarnsholm. We also thank Dr Kimmo Kahma and Dr Heidi Pettersson from the Finnish Institute of Marine Research, Helsinki, Finland for providing the wave buoy data.

## Appendix

### The MIUU turbulence instrument – description and performance

The MIUU instrument, which is shown in Figure A.1, is based on hot wire technology for measurement of the fluctuating wind components, which is standard in wind tunnel studies of turbulent flow, and resistance measurement with platinum sensor for temperature, which is also standard technology. Application of these techniques to measurements in the atmosphere requires, however, that several specific problems must be addressed:

(i) Hot wires are extremely fragile and not very suitable for outdoor work; instead, we have employed hot film probes (DANTEC type 55R02, with $5 \cdot 10^{-7}$ m Ni-film sensor deposited on a $7 \cdot 10^{-5}$ m quartz fibre). They are much more robust but are still fast enough for our application (we sample with 20 hertz, and they can resolve several hundred hertz).

(ii) Wind direction variations are much larger in the atmosphere than in the wind tunnel, and hot film probes (as well as hot wire probes) operate within a limited angle of attack range. We solved this problem by mounting the hot film probes on a wind vane connected to a low-friction potentiometer, which enables recording of the actual orientation of the hot film probes at any moment.

(iii) The output of hot film probes (like hot wire probes) depends on the temperature of the ambient air, which varies within a wide range in the atmosphere. This effect has been taken into account by a calibration procedure briefly described below.



DOI: 10.1002/qj

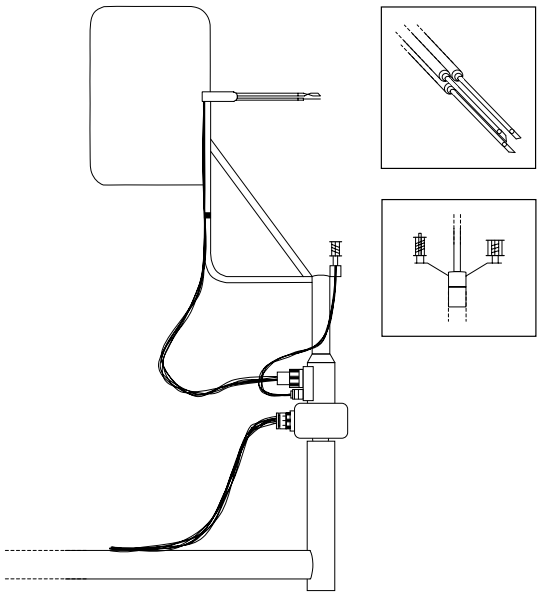

Figure A.1. The MIUU turbulence instrument. The sketch is approximately scale correct, the vertical distance between the hot-film probe head and the supporting boom being 0.66 m.

(iv) Hot film probes (like hot wire probes) require individual calibration. Special technique has been developed, see below.
(v) The structure supporting the hot film probes will inevitably introduce flow distortion. This problem has been thoroughly checked for our measurement configuration (as per Figure A.1) in a big wind tunnel, and the resulting correction is described by a simple analytical expression, see below.
(vi) The platinum sensors for measurement of fluctuating temperature must be thin enough to record fluctuations up to at least 20 hertz and insensitive to heating by direct radiation from the sun. We have demonstrated that $1.5 \cdot 10^{-5}$ m Pt-wire arranged in a particular geometric configuration (see below) meets this criterion.

*Geometrical design and flow distortion*

Optimal geometric design of the instrument is crucial for minimizing flow distortion, item (v) above. The present configuration (Figure A.1) is the result of co-operation with expertise on aerodynamic design at the Department of Aeronautics at the Royal Institute of Technology in Stockholm, Sweden. As described in detail in Högström (1982), the local flow around each part of the instrument was mapped with a sensitive flow direction probe in a big wind tunnel. It was found that flow distortion arises from two parts of the instrument, (a) the vertical cylindrical part ending 0.24 m below the hot film probes and (b) the supporting horizontal boom situated 0.66 m below the probes. This flow distortion is accurately corrected for by the equation:

$$w = -U \sin 0.257^\circ + 0.9012 w_r, \tag{A.1}$$

where $w$ is the correct vertical velocity, $w_r$ the recorded vertical velocity and $U$ the horizontal wind velocity. The first term in Equation (A.1) arises as a result of the horizontal supporting boom, and the second term is due to the vertical cylindrical part of the instrument. The MIUU instrument is equipped with electronic tilt sensors, which enable levelling of the instrument to within $\pm 0.02$ degrees. If not corrected for with Equation (A.1), the flow distortion will give an apparent non-zero mean vertical velocity when the instrument is ideally levelled in the field. As illustrated in Högström (1982), if instead of applying this correction, the mean vertical velocity is simply forced to zero by 'tilt correction', systematic errors of about 20% arise in all second order moments which include the vertical velocity. After application of Equation (A.1) on the measured vertical velocities, computed mean vertical velocities (30-minute means) over flat land are within typically $\pm 0.03$ m s$^{-1}$ (Högström and Bergström, 1996). Note, that when the effect of local flow distortion by the instrument itself has been removed (with Equation A.1), there is no problem to correct for misalignment of the instrument by 'tilt correction'.

*Computation of the wind vector from the hot-film array and calibration procedures*

The MIUU instrument is equipped with three 45° hot film probes, which means that all sensors are inclined by 45° against their horizontally oriented support axis. Two of these probes, which are each $3 \cdot 10^{-3}$ m long, are placed in vertical planes $6.5 \cdot 10^{-3}$ m apart but in such a way that the sensors are at right angles with each other; the third probe is placed with it sensor in the horizontal plane, $3 \cdot 10^{-3}$ m below the other two sensors. Each sensor is placed in a constant temperature bridge, which keeps the operating temperature $T_p = \text{constant} \approx 200\,^\circ\text{C}$. The electronics needed for this is placed in small box ($0.2 \times 0.12 \times 0.06$ m) placed on the supporting boom about 1 m from the instrument. Concerning details of the electronics, see Högström *et al*. (1980). The amount of electric current needed to keep the temperature of the probe constant is strongly dependent on the 'cooling velocity'. This is recorded by measuring the voltage drop over the probe, the resistance of which is kept constant by the electronics. The relation between the 'cooling velocity' $U_c$ and the corresponding voltage output $V$ is called King's law:

$$V^2 = A + B U_c^n, \tag{A.2}$$

where $n \approx 0.43$ and $A$ and $B$ are functions of the so-called overheat ratio

$$\varepsilon = \frac{T - T_0}{T_p - T_0}, \tag{A.3}$$

where $T$ is the ambient temperature, $T_0$ a reference temperature and $T_p$ the probe temperature.



DOI: 10.1002/qj

In Bergström and Högström (1987) it is described in detail how the actual wind vector is computed from the three cooling velocity signals for this particular probe type and probe geometry and how the explicit effect of ambient temperature is taken care of. These calibration results were obtained from experiments with a miniature wind tunnel, Figure A.2, placed in a climate chamber, where the ambient temperature was varied between $-10\,^{\circ}$C and $+30\,^{\circ}$C.

The miniature wind tunnel (Figure A.2) is also used before and after each field experiment to check that the calibration of the particular probes used does not change during the experiment. As seen from Figure A.2, the wind vane is removed and the probes are placed near the centre in the working section of the wind tunnel, which is 0.3 m long and has a diameter of $5{\cdot}10^{-2}$ m. The outlet of the tunnel is connected to a vacuum cleaner, which enables wind velocities in the range 2–20 m s$^{-1}$ in the working section. The wind tunnel flow has very low turbulence level, 0.25%, and a rather flat velocity profile, so that the flow can be considered as uniform over the area subtended by the three probes. A small blocking effect caused by the probe head in the miniature wind tunnel could be derived by comparison with results from measurements in a big wind tunnel; it amounts to about 3.7% and is included in evaluation of the calibration tests.

Taking into account all sources of uncertainty to the calibration of the hot film probes (temperature effect, wind tunnel calibration uncertainty), it is concluded that the wind estimates are expected to have an overall accuracy of about 0.5%. In Högström and Smedman (2004) a field experiment with three MIUU instruments is presented. At a flat low-vegetation site, three MIUU instruments were placed at the same height at 1.56 m above ground on a connecting line oriented 146°–326°. The distance between instrument nos 1 and 2 was 3.1 m and between nos 2 and 3, 1.5 m. The wind direction during the 20 hours of measurements was very steady and nearly perpendicular to the connecting line, $246^{\circ} \pm 6^{\circ}$ (standard deviation of 30-minute means). The mean wind speed at the measuring height during the 20-hour test period was 5.06 m s$^{-1}$. Comparing all simultaneous individual 30-minute wind velocities recorded by the three instruments with each other gave the result that they agree within 0.5%, i.e. exactly the same degree of accuracy predicted from the laboratory calibrations. Below is presented the corresponding result from comparing the sensible heat flux estimates from this experiment.

### *Measurement of temperature fluctuations and flux of sensible heat*

Temperature fluctuations are measured with a $1.5{\cdot}10^{-5}$ m thick platinum wire of about 0.15 m length wound around an array of six $1.5{\cdot}10^{-2}$ m long thin vertical nylon strings, so that the Pt-wire forms a helix of roughly $10^{-2} \times 10^{-2} \times 10^{-2}$ m. Smedman and Lundin (1987) investigated the performance of this sensor in general and its sensitivity to details of the supporting structure in particular. The sensor is operated in a dc Wheatstone bridge circuit with a current of 1 mA. With the high length/diameter ratio (c. $10^4$) the wire temperature overheat is very small and so is also the sensitivity to wind velocity. Two geometric configurations for the supporting structure was tested: (a) the supporting nylon strings were suspended from the circumference of two thin horizontal circular plates, which were held together by a $3{\cdot}10^{-3}$ m diameter plastic cylinder in the middle; (b) the

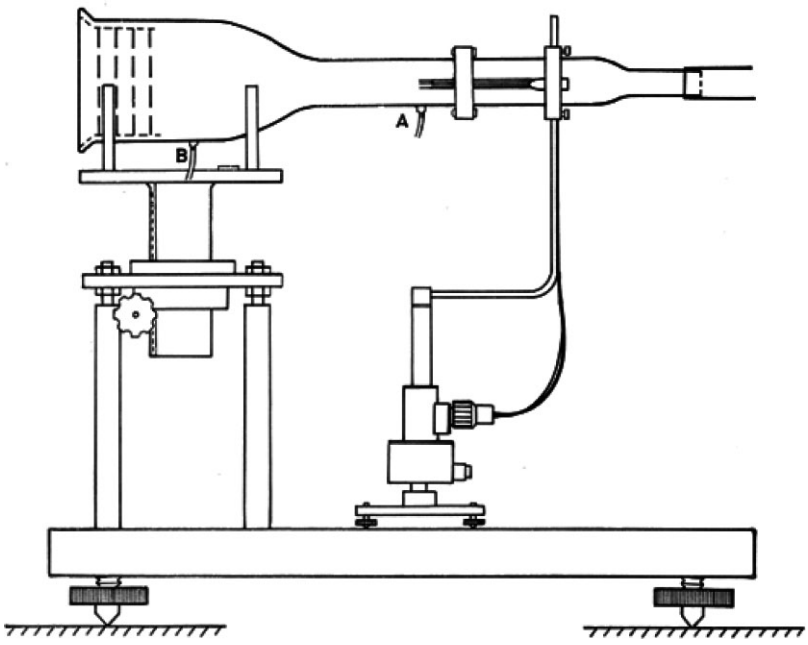


Figure A.2. Calibration wind tunnel for the MIUU instrument with an instrument in calibration position. The inlet of the tunnel is connected to a vacuum cleaner. Tunnel flow velocity is obtained by measuring the pressure difference between points A and B. The sketch is approximately scale correct, the vertical distance between the hot-film probe head and the vertical cylindrical part being 0.24 m.



DOI: 10.1002/qj

central cylinder was removed and the two originally circular plates were changed into an oblong shape, so that two slender supporting rods could be placed outside the helix itself. Field tests of the two types of sensor show unexpected large differences in performance: for sensor (a) spectra start to drop below the expected $-2/3$ slope for n > 1 Hz, whereas spectra measured with sensor (b) follow the expected frequency fall-off very closely to 25 Hz (in this particular test, the sampling frequency was 50 Hz). Thus, the cylindrical support in (a) produces distortions of temperature fluctuations up to a scale $10^3$ times larger than that of the cylinder. Measured noise spectra show that for version (b) the signal-to-noise ratio will be large enough up to 10 Hz during most atmospheric conditions.

Each individual Pt-sensor is calibrated with a technique described in Högström *et al*. (1980), and the resulting reproducibility is quite high. This is illustrated by Figure 4 of Smedman and Lundin (1987), which shows temperature spectra obtained with two sensors of type (b) mounted on a MIUU instrument 0.10 m apart. The plot shows that for each of the 22 spectral points in the spectral range covered, 0.001 < n < 10 Hz, the two sensors give virtually identical values.

The kinematic heat flux $\overline{w'\theta'}$ is derived from the simultaneous signals of vertical velocity, derived from the hot film array, and temperature, derived from the Pt-sensor situated about 0.2 m below the hot film probes. It can be shown that this separation is small enough to be of no concern for determination of the kinematic heat flux for virtually all conditions of interest in this paper, i.e. for wind speed in excess of 2 m $s^{-1}$ and measuring heights well above a metre.

The MIUU parallel test discussed above enables comparison of every desired statistical parameter, see Table II of Högström and Smedman (2004). For the kinematic heat flux, the mean absolute value $\overline{|w'\theta'|}$ (this measure is used because the measurements included both day and night measurements, with positive values during the day and negative values during the night) was 0.042 m $s^{-1}$ K, with a corresponding standard deviation 0.0040 m $s^{-1}$ K, i.e. 9.5% of the mean flux. The kinematic heat flux can be written as the product between the correlation coefficient between the vertical velocity fluctuations and the temperature fluctuations $r_{w\theta}$ and the standard deviation of the vertical velocity $\sigma_w$ and of the temperature fluctuations $\sigma_T$

$$\overline{w'\theta'} = r_{w\theta}\sigma_w\sigma_T. \tag{A.4}$$

The relative error in $\overline{w'\theta'}$ can then be expressed as:

$$(\delta(\overline{w'\theta'})/\overline{w'\theta'})^2 = (\delta(r_{w\theta})/r_{w\theta})^2 + (\delta(\sigma_w)/\sigma_w)^2 + (\delta(\sigma_T)/\sigma_T)^2. \tag{A.5}$$

If we substitute the $\delta$-terms with the corresponding standard deviations taken from Table II of Högström and Smedman (2004), we have: $\delta(\sigma_w)/\sigma_w = 0.033$ and $\delta(\sigma_T)/\sigma_T = 0.063$ and, as noted before, $\delta(\overline{w'\theta'})/\overline{w'\theta'} = 0.095$. Inserting these figures shows that for the uncertainty of the correlation coefficient we have: $\delta(r_{w\theta})/r_{w\theta} = 0.063$. Thus, a roughly 6% error in each of the quantities $\sigma_T$ and $r_{w\theta}$ and 3% error in $\sigma_w$ all contribute to the observed uncertainty in $\overline{w'\theta'}$. Note that a random error of 9.5% in the sensible heat flux measured over typically 30 or 60 minutes is likely to be less than random fluctuations of the mean due to mesoscale variations.

*Concluding remarks*

Above it has been demonstrated how extensive laboratory tests and results from a field inter-comparison test together give convincing evidence of a turbulence instrument with very attractive characteristics. In addition, results from analysis of data obtained with the MIUU instruments during numerous field experiments in a variety of natural environments demonstrate how fundamental theoretical predictions on turbulence structure are validated, like $-2/3$ slope of high-frequency spectra of the wind components and temperature, 5/3 ratio of transverse to longitudinal high-frequency wind component spectra, $-4/3$ slope of *uw* co-spectra, etc. (Högström, 1988, 1990; Högström and Bergström, 1996; Högström *et al*., 2002). Finally, it should be noted that the hot film probes are remarkably weather resistant, and that agreement of pre- and post-campaign calibrations guarantee that no results from possibly malfunctioning probes are erroneously accepted. In fact, the hot film probes never change their characteristics gradually – either they keep their calibrations or, which happens rarely, change abruptly, perhaps as the result of probe contamination from impact of an acid particle (localized blotches are seen under a microscope). The Pt-sensors for measuring temperature fluctuations invariably retain their calibration.

## References


Andreas EL. 2004. 'A bulk air-sea flux algorithm for high-wind, spray conditions, version 2.0.' *Preprints, 13th Conference on Interactions of the Sea and Atmosphere, Portland, ME, 9–13 August 2004*. American Meteorological Society, CD-ROM P1.5, 8 pp.

Bergström H, Högström U. 1987. Calibration of a three-axial fiber-film system for meteorological turbulence measurements. *Dantec Information* **5**: 16–20.

Brunke MA, Fairall CW, Zeng X, Eymard L, Curry JA. 2003. Which bulk aerodynamic algorithms are least problematic in computing ocean surface turbulent fluxes? *J. Climate* **16**: 619–635.

Chang H-R, Grossman RL. 1999. Evaluation of bulk surface flux algorithms for light wind conditions using data from the Coupled Ocean-Atmospheric Response Experiment (COARE). *Q. J. R. Meteorol. Soc.* **125**: 1551–1588.

Clayson CA, Fairall CW, Curry JA. 1996. Evaluation of turbulent fluxes at the ocean surface using surface renewal theory. *J. Geophys. Res.* **101**(C12): 28503–28513.

DeCosmo J, Katsaros KB, Smith SD, Anderson RJ, Oost WA, Bumke K, Chadwick H. 1996. Air-sea exchange of water vapor and sensible heat: the Humidity Exchange Over the Sea (HEXOS) results. *J. Geophys. Res.* **101**(C5): 12001–12016.

Donelan MA. 1990. Air-sea interaction. Pp. 239–292 in *The Sea*, vol. 9, *Ocean Engineering Science*. Wiley-Interscience: New York.

Drennan WM, Graber HC, Hauser D, Quentin C. 2003. On the wave age dependence of wind stress over pure wind seas. *J. Geophys. Res.* **108**(C3): 8062, doi: 10.1029/2000JC000715.

Dupuis H, Taylor PK, Weill A, Katsaros K. 1997. Inertial dissipation method applied to derive turbulent fluxes over the ocean during the SOFIA/ASTEX and SEMAPHORE experiments with low to moderate wind speeds. *J. Geophys. Res.* **102**(C9): 21115–21129.

Edson JB, Zappa CJ, Ware JA, McGillis WR, Hare JE. 2004. Scalar flux profile relationships over the open ocean. *J. Geophys. Res.* **109**: C08S09, doi: 10.1029/2003JC001960.

Eymard L, Caniaux G, Dupuis H, Prieur L, Giordani H, Troadec R, Bessemoulin P, Lachaud G, Bouhours G, Bourras D, Guérin C, Le Borgne P, Brisson A, Marsouin A. 1999. Surface fluxes in the North Atlantic current during CATCH/FASTEX. *Q. J. R. Meteorol. Soc.* **125**: 3563–3599.

Fairall CW, Bradley EF, Godfrey JS, Wick GA, Edson JB, Young GS. 1996a. Cool-skin and warm-layer effects on the sea surface temperature. *J. Geophys. Res.* **101**(C1): 1295–1308.

Fairall CW, Bradley EF, Rogers DP, Edson JB, Young GS. 1996b. Bulk parameterization of air-sea fluxes for Tropical Ocean-Global Atmosphere Coupled-Ocean Atmospheric Response Experiment. *J. Geophys. Res.* **101**(C2): 3747–3764.

Fairall CW, White AB, Edson JB, Hare JE. 1997. Integrated shipboard measurements of the marine boundary layer. *J. Atmos. Oceanic Technol.* **14**: 338–359.

Fairall CW, Bradley EF, Hare JE, Grachev AA, Edson JB. 2003. Bulk parameterization of air–sea fluxes: updates and verification of the COARE algorithm. *J. Climate* **16**: 571–591.

Francey RJ, Garratt JR. 1979. Is an observed wind-speed dependence of AMTEX '75 heat transfer coefficients real? *Boundary-Layer Meteorol.* **16**: 249–260.

Friehe CA, Schmitt KF. 1976. Parameterization of air-sea interface fluxes of sensible heat and moisture by the bulk aerodynamic formulas. *J. Phys. Oceanogr.* **6**: 801–809.

Grelle A, Lindroth A. 1996. Eddy-correlation system for long-term monitoring of fluxes of heat, water vapour and $CO_2$. *Global Change Biol.* **2**: 297–307.

Guo Larsén X. 2003. Climatological characteristics at a marine site in the Baltic Sea proper. In: *Air-Sea Exchange of Momentum and Sensible Heat over the Baltic Sea.* ACTA UNIVERSITATIS UPSALIENSIS (PhD thesis from Department of Earth Sciences, Air and Water Science, Villav. 16 SE-75236, Uppsala, Sweden).

Guo Larsén X, Smedman A-S, Högström U. 2004. Air-sea exchange of sensible heat over the Baltic Sea. *Q. J. R. Meteorol. Soc.* **130**: 519–539.

Högström U. 1982. A critical evaluation of the aerodynamical error of a turbulence instrument. *J. Appl. Meteorol.* **21**: 1838–1844.

Högström U. 1988. Non-dimensional wind and temperature profiles in the atmospheric surface layer. *Boundary-Layer Meteorol.* **42**: 263–270.

Högström U. 1990. Analysis of turbulence structure in the surface layer with a modified similarity formulation for near neutral conditions. *J. Atmos. Sci.* **47**: 1949–1972.

Högström U. 1996. Review of some basic characteristics of the atmospheric surface layer. *Boundary-Layer Meteorol.* **78**: 215–246.

Högström U. 2001. 'Results of turbulence instrument inter-comparison in the field. MIUU Autoflux Report. Department of Earth Sciences, Villavägen 16, SE-75273, Uppsala, Sweden. Also: www.soc.soton.ac.uk/JRD/MET/AUTOFLUX/.

Högström U, Bergström H. 1996. Organized turbulence structures in the near-neutral atmospheric surface layer. *J. Atmos. Sci.* **53**: 2452–2464.

Högström U, Smedman A-S. 2004. Accuracy of sonic anemometers: laminar wind-tunnel calibrations compared to atmospheric *in situ* calibrations against a reference instrument. *Boundary-Layer Meteorol.* **111**: 33–54.

Högström U, Enger L, Knudsen E. 1980. 'A complete system for probing the detailed structure of atmospheric boundary layer flow–. Department of Meteorology, Uppsala, Report no. 60.

Högström U, Hunt JCR, Smedman A-S. 2002. Theory and measurements for turbulence spectra and variances in the atmospheric neutral surface layer. *Boundary-Layer Meteorol.* **103**: 101–124.

Kaimal JC, Gaynor JE. 1991. Another look at sonic thermometry. *Boundary-Layer Meteorol.* **56**: 401–410.

Large WG, Pond S. 1982. Sensible and latent heat flux measurements over the ocean. *J. Phys. Oceanogr.* **12**: 464–482.

Liu WT, Katsaros KB, Businger JA. 1979. Bulk parameterization of air-sea exchanges of heat and water vapor including the molecular constraints at the interface. *J. Atmos. Sci.* **36**: 1722–1735.

Lumley JL, Panofsky HA. 1964. *The structure of atmospheric turbulence*. Interscience Publishers: New York, USA.

Oost WA, Jacobs CMJ, Van Oort C. 2000. Stability effects on heat and moisture fluxes at sea. *Boundary-Layer Meteorol.* **95**: 271–302.

Pedreros R, Dardier G, Dupuis H, Graber HC, Drennan WM, Weill A, Guérin C, Nacass P. 2003. Momentum and heat fluxes via the eddy correlation method on the R/V L'Atalante and an ASIS buoy. *J. Geophys. Res.* **108**(C11): 3339, doi: 10.1029/2002JC001449.

Rutgersson A, Smedman A-S, Högström U. 2001. Use of conventional stability parameters during swell. *J. Geophys. Res.* **106**(C11): 27117–27134.

Sahlée E, Smedman A, Högström U, Rutgersson A. 2007. Bulk exchange coefficient for humidity at sea during unstable and neutral conditions: a re-evaluation based on new field data. *J. Phys. Oceanogr.*, submitted.

Sjöblom A, Smedman A-S. 2003a. Vertical structure in the marine atmospheric boundary layer and its implication for the inertial dissipation method. *Boundary-Layer Meteorol.* **109**: 1–25.

Sjöblom A, Smedman A-S. 2003b. Comparison between eddy-correlation and inertial dissipation methods in the marine atmospheric surface layer. *Boundary-Layer Meteorol.* **110**: 141–164.

Smedman A-S, Högström U. 1973. The Marsta micro-meteorological field project. Profile measurement system and some preliminary data. *Boundary-Layer Meteorol.* **5**: 259–273.

Smedman A-S, Lundin K. 1987. Influence of sensor configuration on measurements of dry and wet bulb temperature fluctuations. *J. Atmos. Oceanic Technol.* **4**: 668–673.

Smedman A-S, Lundin K, Bergström H, Högström U. 1991. A precision kite or balloon-borne mini-sonde for wind and turbulence measurements. *Boundary-Layer Meteorol.* **56**: 295–307.

Smedman A, Högström U, Bergström H, Rutgersson A, Kahma KK, Pettersson H. 1999. A case study of air-sea interaction during swell conditions. *J. Geophys. Res.* **104**(C11): 25833–25851.

Smedman A, Guo Larsén X, Högström U, Kahma KK, Pettersson H. 2003. Effect of sea state on the momentum exchange over the sea during neutral conditions. *J. Geophys. Res.* **108**(C11): 3367, doi: 10.1029/2002JC001526.

Smedman A-S, Högström U, Hunt JCR, Sahlée E. 2007. The changing eddy structure near the surface in unstable close to neutral atmospheric boundary layers and the effects on heat/mass transfer, especially over the ocean. *Q. J. R. Meteorol. Soc.* **133**: [this issue].

Smith SD. 1980. Wind stress and heat flux over the ocean in gale force winds. *J. Phys. Oceanogr.* **10**: 709–726.

Smith SD, Katsaros KB, Oost WA, Mestayer PG. 1996. The impact of the HEXOS programme. *Boundary-Layer Meteorol.* **78**: 121–141.

Weill A, Eymard L, Caniaux G, Hauser D, Planton S, Dupuis H, Brut A, Guerin C, Nacass P, Butet A, Cloché S, Pedreros R, Durand P, Bourras D, Giordani H, Lachaud G, Bouhours G. 2003. Toward a better determination of turbulent air–sea fluxes from several experiments. *J. Climate* **16**: 600–618.

Wu J. 1992. Variation of the heat transfer coefficient with environmental parameters. *J. Phys. Oceanogr.* **22**: 293–300.